International Journal of Solids and Structures 198 (2020) 1–16

Contents lists available at ScienceDirect

International Journal of Solids and Structures

journal homepage: www.elsevier.com/locate/ijsolstr

Pressurized axisymmetric membrane deforming into a prescribed shape

Milan Jirásek*, Filip Šmejkal, Martin Horák

Czech Technical University in Prague, Faculty of Civil Engineering, Department of Mechanics, Thákurova 7, 16629 Prague 6, Czechia

ARTICLE INFO

Article history:
Received 4 May 2019
Revised 14 April 2020
Accepted 15 April 2020

Keywords:
Axisymmetric membrane
Variable thickness
Prescribed shape
Finite differences
Saint Venant-Kirchhoff model
Green-Lagrange strain
Second Piola-Kirchoff stress

ABSTRACT

This paper presents a new approach to the optimal design of an axisymmetric membrane with variable thickness, which has potential applications in the development of active optical elements (liquid lenses). The governing equations are based on the Saint Venant-Kirchhoff material law, which postulates a linear relation between the Green-Lagrange strains and the second Piola-Kirchoff stresses, combined with the exact description of geometric nonlinearity, without any simplifying assumptions. It is shown that the membrane thickness can be designed such that the prestressed membrane subjected to a given uniform liquid pressure deforms into a prescribed rotationally symmetric shape, e.g., a spherical or parabolic cap. For the special but important case of a spherical cap, a closed-form solution is derived. A numerical procedure is developed for the general case, and its high accuracy and efficiency is demonstrated by examples. The sensitivity of the optimal design to material parameters and prestressing displacement is assessed.

1. Introduction

Membrane liquid lenses (Holochip; Optotune; Rawicz and Mikhailenko, 1996; Ren and Wu, 2012; Sugiura and Morita, 1993; Yang et al., 2008; Ren and Wu, 2007; Shaw and Lin, 2007; Li et al., 2011; Fuh et al., 2012a; Mikš et al., 2013; Wang et al., 2014; Liang and Wang, 2016; Hasan et al., 2017) have been one of increasingly popular topics in optics over the past few years. The optical surface of such a lens is formed by a circular elastic membrane subjected to hydrostatic pressure exerted by an optical liquid. If a constant-thickness membrane is used, the resulting deformed shape is not optimal from the optical point of view and suffers from optical aberrations (Pokorný et al., 2017a; 2017b). The optical aberration correction of membrane liquid lenses can be implemented in many different ways (Zhang et al., 2004; Wang et al., 2013; 2014; Hasan et al., 2017; Choi et al., 2011; Fuh et al., 2012b; Liang and Wang, 2016; Du et al., 2016; Santiago-Alvarado et al., 2013; Huang et al., 2016; Ding et al., 2017; Zhao et al., 2015). In the present study, the deformed membrane shape is controlled by designing a suitable variation of the membrane thickness (still preserving axial symmetry). Ideally, the membrane should deform exactly into the prescribed shape, which eliminates the need for other optical members to correct for optical aberrations. This topic has recently received attention, e.g., in Santiago-Alvarado et al. (2013), Huang et al. (2016), Ding et al. (2017) and Zhao et al. (2015).

Santiago-Alvarado et al. (2013) proposed to design the variable thickness such that, already in the undeformed state, the membrane shape would correspond to the previously designed spherical or parabolic surface. The deformed shape under uniform pressure loading was then calculated in Solidworks FEM plugin. Furthermore, the authors investigated optical parameters of the resulting deformed surfaces. With respect to the membrane optimal variable thickness determination, this approach remains a trial-and-error procedure.

Another method was suggested by Huang et al. (2016) who calculated the deformed shape of a constant-thickness membrane under uniform pressure using the COMSOL finite element package. The deformed shape was later used as a thickness profile for a variable-thickness membrane. Again, this approach does not seem to have a theoretical background and can be considered as a trial-and-error method. A similar approach was presented by Ding et al. (2017), who investigated three thickness profiles (spherical concave, spherical convex, constant thickness) and calculated the deformed shape using COMSOL.

Let us now discuss the approach developed by Zhao et al. (2015). Firstly, the authors determined the desired shape of the membrane optical surface using the Code V optical designing software. Secondly, based on a set of two differential equations describing large deflections of circular axisymmetric

* Corresponding author.
E-mail address: milan.jirasek@fsv.cvut.cz (M. Jirásek).

https://doi.org/10.1016/j.ijsolstr.2020.04.021
0020-7683/

slabs (Timoshenko and Woinowsky-Krieger, 1959), they calculated the variable thickness that corresponds to the designed deformed shape, mechanical parameters and loading pressure. Since the designed optical surface typically does not contain any inflection points and the adopted model takes into account the influence of bending stiffness, the solution for the variable thickness tends to zero on the edge boundary (any other value of boundary thickness would result into inflection points close to this boundary). To make the design feasible from the practical point of view, the authors decided to increase the boundary thickness to the minimal feasible value and they approximated the resulting thickness profile by a suitable exponential function with a few parameters that can be changed to optimize the thickness profile later. Furthermore, finite element simulations in ANSYS were performed and the difference between the resulting deformed shape and the designed shape was assessed. The whole process was embedded into an optimization loop, in which the parameters of an exponential function describing the thickness profile were optimized such that the difference between the calculated deformed shape and the designed shape would become as small as possible. The optimization method used by the authors is not clearly explained in this paper but otherwise the whole process is well described.

In most of the above mentioned publications, the numerical methods treating the adopted mechanical models are not exposed in detail. A more elaborate coverage of various applicable numerical methods (power series method, relaxation iterative technique, finite difference method, finite element method) can be found in Hencky (1915), Campbel (1956), Goldberg and Pifko (1963), Pifko and Goldberg (1964), Kao and Perrone (1971), Perrone and Kao (1971), Kelkar et al. (1985), Fichter (1997), Allman (1982), Sheploak and Dugundji (1998), Zhao et al. (2015), Stanford and Ifju (2008) and Mikš and Novák (2014).

The aim of the present paper is to derive and analyze a procedure for a systematic design of the variable membrane thickness profile that leads, for given mechanical parameters and loading by given uniform pressure, to the prescribed deformed shape. The underlying mechanical model is introduced in Section 2 and its mathematical structure is analyzed in detail. A computational approach based on finite differences is presented in Section 3.1 and its performance is illustrated by a numerical example. In Section 4 it is shown that a closed-form solution can be derived for the special case of a spherical cap. Finally, sensitivity of the resulting optimal design to changes of material properties and initial prestress (imposed by prescribing a radial displacement on the boundary) is studied in Section 5.

2. Theoretical prediction of variable-thickness membrane shape

2.1. Derivation of governing equations

Let us consider a circular axisymmetric membrane of a liquid lens, with the axis of symmetry denoted as z and the radial axis as r; see Fig. 1. In the undeformed (stress-free) state, the membrane is characterized by variable thickness $h(r)$ and radius a, with h so small that the bending stiffness can be neglected. Along its circumference, the membrane can generally be displaced (prestressed) in the radial direction by prescribed displacement u_a, which induces an initial prestress. Under applied pressure p of the optical liquid in the lens, the membrane deforms and a general point on its midplane with initial coordinates $[r,0]$ is displaced to a new position $[r+u(r),\, w(r)]$, where $w(r)$ denotes the deflection (displacement in the z-direction) and $u(r)$ is the radial displacement. The deformed shape of the membrane can be characterized by a certain function $g(r)$, implicitly defined by the relation $g(r+u(r)) = w(r)$. The membrane thickness h is considered as very small compared

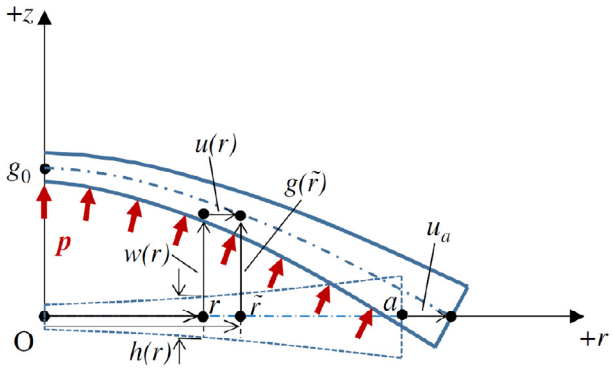

Fig. 1. Sketch of a circular axisymmetric membrane deformed by constant liquid pressure p (dashed blue lines – initial straight shape of the prestressed membrane at zero applied pressure, $w(r)$ and $u(r)$ – vertical and horizontal displacements of a point with initial coordinates $[r,0]$, $\tilde{r}(r) = r + u(r)$ – horizontal coordinate in deformed shape, $g(\tilde{r})$ – prescribed deformed shape, a – membrane radius, $h(r)$ – membrane thickness, g_0 – maximum deflection, u_a – prestressing displacement)

to the deflection, and so the deformed shape is determined by the midsurface. It is also assumed that strains and stresses are uniformly distributed across the thickness of the membrane, which means that bending effects are neglected.

The radial stretch λ_r and the tangential (circumferential) stretch λ_t in the deformed state are easily expressed as

$$\lambda_r = \sqrt{(1+u')^2 + w'^2} \tag{2.1}$$

$$\lambda_t = 1 + \frac{u}{r} \tag{2.2}$$

where u' and w' are the derivatives of displacements u and w with respect to the radial coordinate, r. The corresponding in-plane normal components of the Green-Lagrange strain tensor are evaluated from the stretches as

$$\varepsilon_r = \tfrac{1}{2}(\lambda_r^2 - 1) = u' + \tfrac{1}{2}(u'^2 + w'^2) \tag{2.3}$$

$$\varepsilon_t = \tfrac{1}{2}(\lambda_t^2 - 1) = \frac{u}{r} + \frac{u^2}{2r^2} \tag{2.4}$$

Let us assume that the material can be described by the Saint Venant-Kirchhoff model, which postulates a linear relation between the Green-Lagrange strain and the second Piola-Kirchhoff stress (Audoly and Pomeau, 2010) and is the simplest hyperelastic material model. In Pokorný et al. (2017a,b) it was shown that, despite its simplicity, this model applied to analysis of membranes of a constant thickness leads to a very good agreement with experimentally measured deflections for materials typically used for liquid lenses, such as Sylgard (Sylgard, 184; Johnston et al., 2014).

Since the state of the material corresponds to plane stress, the strain energy density $\mathcal{E}_{\text{int}}$ (per unit volume in the stress-free state) is given by (Timoshenko and Woinowsky-Krieger, 1959; Volmir, 1967)

$$\mathcal{E}_{\text{int}}(\varepsilon_r, \varepsilon_t) = \frac{E}{2(1-\nu^2)}(\varepsilon_r^2 + 2\nu\varepsilon_r\varepsilon_t + \varepsilon_t^2) \tag{2.5}$$

where E is the Young modulus and ν is the Poisson ratio characterizing the membrane material. The expression in (2.5) does not contain the out-of-plane normal strain but this does not mean that this strain component is assumed to be zero—it has been eliminated based on the assumption that the out-of-plane stress is zero. Differentiating the strain energy density with respect to strains, we get the corresponding work-conjugate stresses

$$\sigma_r = \frac{\partial \mathcal{E}_{\text{int}}}{\partial \varepsilon_r} = \frac{E}{1-\nu^2}(\varepsilon_r + \nu\varepsilon_t) \tag{2.6}$$

$$\sigma_t = \frac{\partial \mathcal{E}_{\text{int}}}{\partial \varepsilon_t} = \frac{E}{1-\nu^2}(\varepsilon_t + \nu \varepsilon_r) \tag{2.7}$$

The strain energy density has been differentiated with respect to Green-Lagrange strains, and so the resulting stresses are the second Piola-Kirchhoff stresses. It is important to realize that symbols a and $h(r)$ denote the membrane radius and thickness in the initial undeformed state (i.e., before application of possible prestress caused by imposed radial displacement u_a, and before application of the liquid pressure).

The equilibrium state after application of in-plane prestress and lateral pressure p can be found by exploiting the principle of minimum potential energy. The total potential energy,

$$E_p = E_{\text{int}} + E_{\text{ext}} \tag{2.8}$$

is the sum of the strain energy, E_{int}, and the energy of external forces, E_{ext}. The strain energy

$$E_{\text{int}} = 2\pi \int_0^a \mathcal{E}_{\text{int}}\, h\, r\, \mathrm{d}r \tag{2.9}$$

is obtained by integrating the strain energy density specified in (2.5) over the initial volume of the membrane. The energy of external forces can be expressed as minus the applied pressure multiplied by the volume between the initial midplane and the deformed midsurface, which leads to

$$E_{\text{ext}} = -2\pi\, p \int_0^a w(r+u)(1+u')\, \mathrm{d}r \tag{2.10}$$

The state of minimum potential energy is attained only if the variation of functional E_p vanishes for all admissible variations of displacements u and w. The first variations of the strain energy and of the energy of external forces are evaluated as

$$\begin{aligned}
\delta E_{\text{int}} &= 2\pi \int_0^a \left(\frac{\partial \mathcal{E}_{\text{int}}}{\partial \varepsilon_r}\, \delta\varepsilon_r + \frac{\partial \mathcal{E}_{\text{int}}}{\partial \varepsilon_t}\, \delta\varepsilon_t \right) h\, r\, \mathrm{d}r \\
&= 2\pi \int_0^a (\sigma_r\, \delta\varepsilon_r + \sigma_t\, \delta\varepsilon_t)\, h\, r\, \mathrm{d}r \\
&= 2\pi \int_0^a \Big(h\, r\, \sigma_r\, (\delta u' + u' \delta u' + w' \delta w') + h \sigma_t\, (\delta u + u\, \delta u / r) \Big) \mathrm{d}r \\
&= 2\pi \Big[hr\sigma_r \big(\delta u + u' \delta u + w' \delta w \big) \Big]_{r=0}^{a} \\
&\quad -2\pi \int_0^a \Big(\big(hr\sigma_r (1+u') \big)' \delta u + \big(hr\sigma_r w' \big)' \delta w \Big) \mathrm{d}r \\
&\quad +2\pi \int_0^a h\sigma_t \left(\delta u + \frac{u \delta u}{r} \right) \mathrm{d}r
\end{aligned} \tag{2.11}$$

and

$$\begin{aligned}
\delta E_{\text{ext}} &= -2\pi\, p \int_0^a (r+u)(1+u') \delta w \mathrm{d}r \\
&\quad -2\pi\, p [w(r+u)\delta u]_{r=0}^{a} + 2\pi\, p \int_0^a w'(r+u) \delta u \mathrm{d}r
\end{aligned} \tag{2.12}$$

As shown in Fig. 1, admissible functions u and w are constrained by boundary conditions

$$u(a) = u_a,\ w(a) = 0 \tag{2.13}$$

and by the condition

$$u(0) = 0 \tag{2.14}$$

which follows from displacement continuity and axial symmetry. In fact, functions that do not satisfy (2.14) would not lead to a finite value of strain energy. Variations δu and δw of admissible functions must satisfy conditions

$$\delta u(a) = 0,\ \delta w(a) = 0,\ \delta u(0) = 0 \tag{2.15}$$

Summing (2.11) and (2.12) and making use of conditions (2.15), we obtain the variation of total potential energy in the form

$$\begin{aligned}
\delta E_p = \delta E_{\text{int}} + \delta E_{\text{ext}} &= -2\pi\, hr\sigma_r w' \delta w|_{r=0} \\
&\quad +2\pi \int_0^a \left(h\sigma_t \left(1 + \frac{u}{r} \right) - \big(hr\sigma_r (1+u') \big)' + p w' (r+u) \right) \delta u \mathrm{d}r \\
&\quad -2\pi \int_0^a \Big(\big(hr\sigma_r w' \big)' + p(r+u)(1+u') \Big) \delta w \mathrm{d}r
\end{aligned} \tag{2.16}$$

The corresponding strong form of equilibrium equations reads

$$\big(hr\sigma_r\, (1+u') \big)' - h\sigma_t \left(1 + \frac{u}{r} \right) = p(r+u) w' \tag{2.17}$$

$$-(hr\sigma_r w')' = p(r+u)(1+u') \tag{2.18}$$

Since the variation δw at $r = 0$ is arbitrary, the first term on the right-hand side of (2.16) leads to the boundary condition

$$hr\sigma_r w' = 0 \qquad \text{at } r = 0 \tag{2.19}$$

At a first glance, the condition seems to be satisfied automatically. Indeed, if $\sigma_r w'$ has a finite value at $r = 0$, then multiplication by zero leads to $r\sigma_r w' = 0$. In a general case, a concentrated vertical force F_0 could be applied at $r = 0$ and then the resulting boundary condition would read $\lim_{r\to 0^+} (hr\sigma_r w') = F_0/(2\pi)$. For the problem studied here, no such concentrated force is present, and condition (2.19) is rewritten more carefully as

$$\lim_{r \to 0^+} (hr\sigma_r w') = 0 \tag{2.20}$$

In this form, we admit that $h\sigma_r w'$ might tend to infinity but its growth must be slower than $1/r$.

Two differential equations (2.17)–(2.18) contain three functions, $h(r)$, $u(r)$ and $w(r)$. If one of these functions is prescribed, the other two can be computed, provided that we know the mechanical parameters of membrane material, the dimensions and loading pressure p. In a standard setting, the membrane thickness $h(r)$ is prescribed and displacements $u(r)$ and $w(r)$ are treated as unknown functions. However, in the present context of optimal design of a liquid lens, we consider the thickness $h(r)$ as unknown and we prescribe a desired shape of the deformed membrane. The deformed shape is affected by $u(r)$ as well as by $w(r)$, and so neither of these functions is given directly. Instead, prescribing the deformed shape leads to the constraint equation

$$w(r) = g(r + u(r)) \tag{2.21}$$

which provides a link between functions $u(r)$ and $w(r)$. Here, $g(\tilde{r})$ is a given function that describes how the deflection should depend on the radial coordinate in the deformed configuration, $\tilde{r} = r + u(r)$; see Fig. 1. Our objective is to find the function $h(r)$ such that the deformed shape calculated for the specific values of material parameters E and ν and hydrostatic pressure p satisfies condition (2.21).

Let us first eliminate the deflection function $w(r)$ from the governing equations, by making use of condition (2.21). Integrating (2.18) with boundary condition (2.20) we obtain

$$hr\sigma_r w' = -\tfrac{1}{2} p (r+u)^2 \tag{2.22}$$

Based on condition (2.21), the derivative of w can be expressed as

$$w'(r) = (1 + u'(r)) g'(r + u(r)) \tag{2.23}$$

To simplify notation, we will write this relation without explicitly specifying the arguments, i.e., as

$$w' = (1 + u') g' \tag{2.24}$$

but it should be borne in mind that g' has to be evaluated at $r + u$ and not at r. The same convention will later be used for the second derivative, g''.

Using (2.24) in (2.22) yields

$$hr\sigma_r = -\frac{p(r+u)^2}{2(1+u')g'} \tag{2.25}$$

and the first term on the left-hand side of (2.17) can now be expressed as

$$\begin{aligned}\big(hr\sigma_r(1+u')\big)' &= -\frac{p}{2}\left(\frac{(r+u)^2}{g'}\right)' \\ &= p(r+u)(1+u')\left(\frac{(r+u)g''}{2g'^2} - \frac{1}{g'}\right)\end{aligned} \tag{2.26}$$

The tangential stress σ_t is then evaluated from (2.17) as

$$\begin{aligned}\sigma_t &= \frac{r}{(r+u)h}\big[(hr\sigma_r\,(1+u'))' - p(r+u)(1+u')g'\big] = \\ &= \frac{pr}{h}(1+u')\left(\frac{(r+u)g''}{2g'^2} - \frac{1}{g'} - g'\right)\end{aligned} \tag{2.27}$$

and, according to (2.25), the radial stress is given by

$$\sigma_r = -\frac{p(r+u)^2}{2hr(1+u')g'} = -\frac{pr}{h}\frac{(r+u)^2}{2r^2(1+u')g'} \tag{2.28}$$

By inversion of constitutive equations (2.6)–(2.7), strains are expressed as

$$\varepsilon_r = \frac{pr}{Eh}\left[-\frac{(r+u)^2}{2r^2(1+u')g'} - \nu(1+u')\left(\frac{(r+u)g''}{2g'^2} - \frac{1}{g'} - g'\right)\right] \tag{2.29}$$

$$\varepsilon_t = \frac{pr}{Eh}\left[\nu\frac{(r+u)^2}{2r^2(1+u')g'} + (1+u')\left(\frac{(r+u)g''}{2g'^2} - \frac{1}{g'} - g'\right)\right] \tag{2.30}$$

and substitution into the strain-displacement equations (2.3)-(2.4) yields

$$\begin{aligned}&\frac{pr}{Eh}\left[-\frac{(r+u)^2}{2r^2(1+u')g'} - \nu(1+u')\left(\frac{(r+u)g''}{2g'^2} - \frac{1}{g'} - g'\right)\right] \\ &= u' + \tfrac{1}{2}(u'^2 + (1+u')^2g'^2)\,,\end{aligned} \tag{2.31}$$

$$\begin{aligned}&\frac{pr}{Eh}\left[\nu\frac{(r+u)^2}{2r^2(1+u')g'} + (1+u')\left(\frac{(r+u)g''}{2g'^2} - \frac{1}{g'} - g'\right)\right] \\ &= \frac{u}{r} + \frac{u^2}{2r^2}\end{aligned} \tag{2.32}$$

This is a set of two equations for unknown functions u and h, but h is involved only algebraically and can easily be eliminated. The resulting first-order differential equation for unknown function u reads

$$\begin{aligned}&\left[\frac{(r+u)^2}{2r^2g'} + \nu(1+u')^2\left(\frac{(r+u)g''}{2g'^2} - \frac{1}{g'} - g'\right)\right]\left(\frac{u}{r} + \frac{u^2}{2r^2}\right) \\ &+\left[\nu\frac{(r+u)^2}{2r^2g'} + (1+u')^2\left(\frac{(r+u)g''}{2g'^2} - \frac{1}{g'} - g'\right)\right] \\ &\left(u' + \tfrac{1}{2}u'^2 + \tfrac{1}{2}(1+u')^2g'^2\right) = 0\end{aligned} \tag{2.33}$$

and its solution should satisfy the first condition in (2.13) and also condition (2.14). Once the displacement function is determined, the thickness function h can be calculated from (2.31) as

$$h = \frac{pr}{E} \times \frac{\nu(1+u')\left(g' + \frac{1}{g'} - \frac{(r+u)g''}{2g'^2}\right) - \frac{(r+u)^2}{2r^2(1+u')g'}}{u' + \frac{1}{2}(u'^2 + (1+u')^2g'^2)} \tag{2.34}$$

An alternative formula could be obtained from (2.32) but it would provide the same results.

2.2. Mathematical structure of the problem

In the previous section, we have derived Eq. (2.33), which can be used together with (2.34) to find the membrane thickness distribution $h(r)$ that will lead, under pressure p, to the prescribed deformed shape $g(\tilde{r})$. Differential equation (2.33) has certain special features and deserves a deeper analysis before we proceed to a numerical scheme. First of all, the equation is not only highly nonlinear, but it does not even have the standard form $u' = F(u, r)$, which would permit a direct evaluation of the derivative $u' \equiv \mathrm{d}u/\mathrm{d}r$ from the values of u and r. Instead of that, the equation is presented in an implicit form, $F(u', u, r) = 0$, and even if the value of u at point r is known, the corresponding derivative u' must be computed by solving a nonlinear algebraic equation. In terms of u', function F is a fourth-order polynomial, and therefore a unique solution cannot be expected.

Luckily, it turns out that u' can be found analytically, because Eq. (2.33) can be reformulated as a quadratic equation in terms of a transformed unknown, defined as

$$\eta = (1+u')^2 \tag{2.35}$$

Based on this transformation, all terms $(1+u')^2$ in (2.33) are replaced by η, and the expression $u' + u'^2/2$ is replaced by $(\eta - 1)/2$. If the whole equation is then multiplied by $4g'^2$ and divided by $(r+u)g'' - 2g' - 2g'^3$, the resulting quadratic equation can be presented in the form

$$A(u,r)\,\eta^2 + B(u,r)\,\eta + C(u,r) = 0 \tag{2.36}$$

where

$$A(u,r) = 1 + g'^2 \tag{2.37}$$

$$B(u,r) = \frac{2\nu u}{r} + \frac{\nu u^2}{r^2} - 1 + \nu(1+g'^2)\alpha(u,r) \tag{2.38}$$

$$C(u,r) = \left(\frac{2u}{r} + \frac{u^2}{r^2} - \nu\right)\alpha(u,r) \tag{2.39}$$

are coefficients and

$$\alpha(u,r) = \frac{\left(1+\frac{u}{r}\right)^2 g'}{(r+u)g'' - 2g' - 2g'^3} \tag{2.40}$$

is an auxiliary function, introduced for convenience.

If the discriminant $D = B^2 - 4AC$ is positive, Eq. (2.36) has two real roots,

$$\eta_{1,2}(u,r) = \frac{-B(u,r) \pm \sqrt{B^2(u,r) - 4A(u,r)C(u,r)}}{2A(u,r)} \tag{2.41}$$

and if both of these roots are positive, the original Eq. (2.33) has four real roots, which can be symbolically presented as

$$u'_{1,2,3,4} = \pm\sqrt{\eta_{1,2}} - 1 \tag{2.42}$$

Intuitively it can be expected that only one of these roots corresponds to a physically meaningful solution. To get more insight, let us work out a specific example.

2.3. Example: Parabolic cap (part I)

Consider a membrane of radius $a = 9$ mm (in the undeformed state). The membrane is prestressed by imposing an initial radial displacement $u_a = 1$ mm on the outer boundary, i.e., its radius is increased to $a_p = a + u_a = 10$ mm. Furthermore, suppose that the desired deformed shape is an axisymmetric parabolic cap, described by

$$g(\tilde{r}) = \left(1 - \frac{\tilde{r}^2}{(a+u_a)^2}\right)g_0 = \left(1 - \frac{\tilde{r}^2}{a_p^2}\right)g_0 \tag{2.43}$$

where $g_0 = g(0) = 3$ mm is the given deflection at the center, and $\tilde{r}$ is the radial coordinate in the deformed configuration, running from 0 to a_p. The derivatives of g are easily expressed as

$$g'(\tilde{r}) \equiv \frac{\mathrm{d}g(\tilde{r})}{\mathrm{d}\tilde{r}} = -\frac{2g_0\tilde{r}}{a_p^2} \tag{2.44}$$

$$g''(\tilde{r}) \equiv \frac{\mathrm{d}^2g(\tilde{r})}{\mathrm{d}\tilde{r}^2} = -\frac{2g_0}{a_p^2} \tag{2.45}$$

Let us now set up Eq. (2.36) at $r = a$ and $u = u_a$, so that the value of $u'(a)$ can be determined. The values of g' and g'' that are substituted into (2.37)–(2.40) correspond to $\tilde{r} = r + u = a + u_a = a_p$ and are given by $g' = -2g_0/a_p$ and $g'' = -2g_0/a_p^2$. Formulae (2.40) and (2.37)–(2.39) now yield

$$\alpha(u_a, a) = -\frac{-\dfrac{2g_0a_p}{a^2}}{-\dfrac{2g_0}{a_p} + \dfrac{4g_0}{a_p} + \dfrac{16g_0^3}{a_p^3}} = -\frac{a_p^2}{a^2(1 + 8g_0^2/a_p^2)} \tag{2.46}$$

and

$$A(u_a, a) = 1 + \frac{4g_0^2}{a_p^2} \tag{2.47}$$

$$B(u_a, a) = \nu\frac{a_p^2}{a^2} - \nu - 1 + \nu\left(1 + \frac{4g_0^2}{a_p^2}\right)\alpha(u_a, a) \tag{2.48}$$

$$C(u_a, a) = \left(\frac{a_p^2}{a^2} - 1 - \nu\right)\alpha(u_a, a) \tag{2.49}$$

Substituting $\nu = 0.4$, $g_0/a_p = 0.3$ and $a_p/a = 10/9$, we obtain $\alpha = -0.71777$, $A = 1.36$, $B = -1.2966$ and $C = 0.1187$. The discriminant $D = 1.0353$ is positive and the roots of (2.36), $\eta_1 = 0.85079$ and $\eta_2 = 0.10262$, are also positive. Therefore, the original Eq. (2.33) has four solutions, $u_1' = \sqrt{\eta_1} - 1 = -0.07762$, $u_2' = \sqrt{\eta_2} - 1 = -0.67965$, $u_3' = -\sqrt{\eta_1} - 1 = -1.92238$ and $u_4' = -\sqrt{\eta_2} - 1 = -1.32035$.

Now we need to determine which of these four solutions that all satisfy Eq. (2.33) is physically meaningful. First of all, we will look at the corresponding values of membrane thickness at $r = a$, which are according to (2.34) evaluated as

$$h(a) = \frac{pa}{E}\frac{1}{u' + 0.5u'^2 + 0.18(1 + u')^2}\left(\frac{1}{0.972(1 + u')} - 0.57333(1 + u')\right) \tag{2.50}$$

For the four possible values of u' listed above, the respective dimensionless factors that multiply pa/E in (2.50) are 7.5231, −7.0441, −7.5231 and 7.0441. Roots u_2' and u_3' would lead to a negative thickness can be excluded from consideration. The other two roots, $u_1' = -0.07762$ and $u_4' = -1.32035$, are retained as candidates for a physically meaningful solution. Root u_4' is smaller than −1, which means that $1 + u_4'$ would be negative and, according to (2.24), the sign of w' would differ from the sign of g'. This corresponds to a parasitic solution for which the membrane would be stretched from the outer support to the external part of the paraboloid described by (2.43), with $\tilde{r} > a_p$. Such a solution is not what we are aiming at. Later it will be shown that, when prolongated, this solution would not satisfy condition $u(0) = 0$. Therefore, $u_1' = -0.07762$ is the only root that leads to a physically admissible solution.

It is natural to ask the question whether the problem always admits exactly one physically admissible solution. Of course, to guarantee uniqueness, certain assumptions or constraints are needed. In quadratic equation (2.36), the leading coefficient A given by (2.37) is always positive, and so the equation has one positive root if $C < 0$ and two positive roots if $0 < C < B^2/(4A)$ and $B < 0$. The sign of coefficient C given by (2.39) is affected by the sign of the auxiliary factor α introduced in (2.40). The sign of α corresponds to the sign of the expression $\tilde{r}g''/g' - 2 - 2g'^2$. Let us first consider the special case of a parabolic cap, for which $g' = \tilde{r}g''$, and so

$$\frac{\tilde{r}g''}{g'} - 2 - 2g'^2 = -1 - g'^2 < 0 \tag{2.51}$$

In a general case, α is negative if the shape-defining function g satisfies the condition

$$g'' > \frac{2(g' + g'^3)}{\tilde{r}} \tag{2.52}$$

Since usually $g' < 0$ and $g'' < 0$, this condition means that the prescribed shape must not be "too curved".

Once we know that α is negative, we can evaluate

$$\operatorname{sgn} C = \operatorname{sgn}(2\varepsilon_t - \nu)\operatorname{sgn}\alpha = \operatorname{sgn}(\nu - 2\varepsilon_t) \tag{2.53}$$

For convenience, we have exploited the strain-displacement Eq. (2.4) and replaced $2u/r + u^2/r^2$ in formula (2.39) by $2\varepsilon_t$, which permits a physical interpretation of the result. Since ε_t represents the circumferential strain, it is typically small. As long as $\varepsilon_t < \nu/2$, coefficient C is positive, and Eq. (2.36) has either 2 or 0 positive roots. A necessary condition for the existence of two positive roots is then $B < 0$, which can be rewritten as

$$\nu\big(2\varepsilon_t + (1 + g'^2)\alpha\big) < 1 \tag{2.54}$$

Since we already assume that $\varepsilon_t < \nu/2$, which is needed to get $\alpha < 0$, the left-hand side of (2.54) is smaller than ν^2 and the condition is satisfied.

To guarantee the existence of two positive roots, one still needs to check that the discriminant $D = B^2 - 4AC$ is positive. This leads to the inequality

$$(1 - 2\nu\varepsilon_t)^2 + \alpha^2\nu^2(1 + g'^2)^2 + 2\alpha(1 + g'^2)[\nu + 2(\nu^2 - 2)\varepsilon_t] > 0 \tag{2.55}$$

in which

$$\alpha = \frac{1}{\tilde{r}g''/g' - 2 - 2g'^2}\frac{\tilde{r}^2}{r^2} \tag{2.56}$$

For $\varepsilon_t = 0$, condition (2.55) is always satisfied. If all other variables are fixed, the left-hand side of (2.55) is a quadratic function of ε_t with a positive second derivative. It is thus sufficient to show that the first derivative evaluated at $\varepsilon_t = 0$ is positive, which leads to the inequality

$$\alpha(1 + g'^2)(\nu^2 - 2) > \nu \tag{2.57}$$

Replacing α by the right-hand side of (2.56), we would obtain a rather complicated condition, which is not easy to analyze in full generality. In the special case of a prescribed parabolic cap we have

$$\alpha = -\frac{1}{1 + 2g'^2}\frac{\tilde{r}^2}{r^2} \tag{2.58}$$

and condition (2.57) can be rewritten as

$$\frac{\tilde{r}^2}{r^2} > \frac{\nu}{2 - \nu^2}\frac{1 + 2g'^2}{1 + g'^2} \tag{2.59}$$

For $u \geq 0$, the left-hand side is not smaller than 1. Since $\nu \leq 0.5$, the right-hand side is smaller than 4/7, and so the condition is satisfied, which means that the discriminant is positive and Eq. (2.36) has two positive roots. Note that $u \geq 0$ is equivalent to $\varepsilon_t \geq 0$.

In summary, we have proven that, for the prescribed parabolic cap and for circumferential strains in the range $0 \leq \varepsilon_t \leq \nu/2$,

Eq. (2.36) has two positive roots, η_1 and η_2. Among the four corresponding roots of Eq. (2.33), those that are smaller than -1 can be excluded, for reasons that have already been explained. Therefore, we only need to consider $u'_1 = \sqrt{\eta_1} - 1$ and $u'_2 = \sqrt{\eta_2} - 1$ as potential solutions. Their physical admissibility should be assessed based on the sign of the corresponding membrane thickness h evaluated from (2.34). In our example, we have shown that one of these roots leads to positive thickness and the other to negative thickness. In fact, since we always consider only the roots for which $u' = \sqrt{\eta} - 1$, formula (2.34) for the membrane thickness can be rewritten in terms of variable η as

$$h = \frac{pr}{E} \times \frac{2}{\eta - 1 + \eta g'^2} \times \left[-\frac{\tilde{r}^2}{2r^2\sqrt{\eta} g'} - \nu\sqrt{\eta}\left(\frac{\tilde{r} g''}{2g'^2} - \frac{1}{g'} - g' \right) \right]$$
$$= -\frac{p\tilde{r}^2}{Erg'\sqrt{\eta}} \times \frac{1}{(1+g'^2)\eta - 1} \times \left(1 + \frac{\nu\eta}{\alpha} \right) \tag{2.60}$$

Since $g' < 0$ for all $\tilde{r} > 0$, the thickness is positive if expressions $(1+g'^2)\eta - 1$ and $1 + \nu\eta/\alpha$ have the same sign. Restricting attention to cases in which $\alpha < 0$, we can write the resulting condition for the selection of the physically meaningful solution in the form

$$\min\left(\frac{1}{1+g'^2}, -\frac{\alpha}{\nu} \right) < \eta < \max\left(\frac{1}{1+g'^2}, -\frac{\alpha}{\nu} \right) \tag{2.61}$$

For the specific data treated in our illustrative example, we have $1/(1+g'^2) = 1/1.36 = 0.735$ and $-\alpha/\nu = 0.71777/0.4 = 1.794$. Therefore, the solution is admissible if $0.735 < \eta < 1.794$, and the correct root is $\eta_1 = 0.85079$, while $\eta_2 = 0.10262$ should be excluded. This confirms that $u'_1 = \sqrt{\eta_1} - 1 = -0.07762$ should be selected as the physically meaningful solution.

We have demonstrated that even though the differential equation to be solved is written in an implicit form $F(u', u, r) = 0$, the derivative u' can be uniquely determined from given values of r and u, provided that the prescribed shape satisfies a certain constraint and the circumferential strain does not exceed $\nu/2$. The reasoning leading to this conclusion was based on an auxiliary quadratic Eq. (2.36) with coefficients given by (2.37)–(2.39). Special attention needs to be paid to the point with coordinate $r = 0$, because coefficients B and C cannot be directly evaluated from formulae (2.38) and (2.39), which contain fractions u/r. Undetermined expressions are also found in formula (2.40) for the auxiliary factor α that needs to be substituted into (2.38) and (2.39).

Under certain assumptions it is possible to obtain finite limits of $\alpha(u(r), r)$, $B(u(r), r)$ and $C(u(r), r)$ for r approaching zero. The assumptions are that u/r tends to a finite limit,

$$\varepsilon_0 = \lim_{r\to 0^+} \frac{u(r)}{r} \tag{2.62}$$

and that the prescribed shape satisfies conditions $g'(0) = 0$ and $g''(0) = g''_0 \neq 0$. Recall that g' and g'' must be evaluated at $\tilde{r} = r + u$ and not at r. This needs to be taken into account when expressing the limit of the fraction $(r+u)/g'$, which would be written in careful notation as

$$\lim_{r\to 0^+} \frac{r + u(r)}{g'(r + u(r))} = \frac{1}{g''(0)} = \frac{1}{g''_0} \tag{2.63}$$

Based on (2.62)–(2.63) and on the assumed properties of function g, it is easy to evaluate

$$\lim_{r\to 0^+} \alpha(u(r), r)$$
$$= \frac{\lim_{r\to 0^+} \left(1 + \frac{u(r)}{r} \right)^2}{\lim_{r\to 0^+} \left[\frac{(r+u(r))g''(r+u(r))}{g'(r+u(r))} - 2 - 2g'^2(r+u(r)) \right]}$$
$$= \frac{(1+\varepsilon_0)^2}{(1-2-0)} = -(1+\varepsilon_0)^2 \tag{2.64}$$

$$\lim_{r\to 0^+} B(u(r), r) = 2\nu\varepsilon_0 + \nu\varepsilon_0^2 - 1 - \nu(1+\varepsilon_0)^2 = -1 - \nu \tag{2.65}$$

$$\lim_{r\to 0^+} C(u(r), r) = -\big(2\varepsilon_0 + \varepsilon_0^2 - \nu\big)(1+\varepsilon_0)^2$$
$$= (1+\nu)(1+\varepsilon_0)^2 - (1+\varepsilon_0)^4 \tag{2.66}$$

Coefficient $A(0, 0) = 1$ can be evaluated by direct substitution into (2.37). Quadratic equation (2.36) written at $r = 0$ and $u = 0$ thus reads

$$\eta^2 - (1+\nu)\eta + (1+\nu)(1+\varepsilon_0)^2 - (1+\varepsilon_0)^4 = 0 \tag{2.67}$$

and it has two real roots,

$$\eta_1 = (1+\varepsilon_0)^2 \tag{2.68}$$

$$\eta_2 = 1 + \nu - (1+\varepsilon_0)^2 \tag{2.69}$$

Root η_1 is always positive, and η_2 is positive if $\varepsilon_0 < \sqrt{1+\nu} - 1$. Admissibility condition (2.61) reads

$$1 < \eta < \frac{(1+\varepsilon_0)^2}{\nu} \tag{2.70}$$

and it is easy to see that η_1 is always admissible while η_2 is not. Interestingly, the resulting admissible solution for u' is $u'_1 = \sqrt{\eta_1} - 1 = \varepsilon_0$ (of course, provided that $\varepsilon_0 > -1$, which is quite natural).

The foregoing analysis is mathematically correct but its physical interpretation is somewhat tricky. In order to evaluate coefficients of quadratic Eq. (2.67) and to calculate the derivative u' at $r = 0$, we had to make the assumption that we know ε_0 defined in (2.62). The calculation then resulted into the conclusion that $u'(0) = \varepsilon_0$. But this should not be so surprising, since the right-hand side of (2.62) in fact represents the derivative of u at $r = 0$ (we have assumed that the limit is finite, which is only possible if $u(0) = 0$, and then the numerator can also be written as $u(r) - u(0)$). Therefore, the analysis does not really show how to compute $u'(0)$ without knowing it beforehand. Still, it is not worthless, because it reveals a special property of differential equation (2.33). Even though we know the value of $u = 0$ at point $r = 0$, the corresponding derivative u' cannot be determined from $F(u', 0, 0) = 0$. The equation can be satisfied in the limit sense for an arbitrary value of u' greater than -1.

3. Computational approach

3.1. Adopted numerical scheme

The intriguing result obtained in the previous example is closely related to another peculiar feature of the problem at hand. After elimination of unknown functions w and h, we ended up with differential equation (2.33) for the remaining unknown function, u. It is unusual that the equation is of the first order but the solution should satisfy two boundary conditions, $u(0) = 0$ and $u(a) = u_a$. It might seem that the problem is overdetermined and there is a danger that no solution exists. Normally, one could use $u(0) = 0$ as the initial condition and integrate the governing first-order differential equation, e.g., by using the forward Euler scheme. This procedure would provide the entire function $u(r)$, including the value of $u(a)$. But then, the boundary condition $u(a) = u_a$ would be satisfied only by chance, for one particular value of u_a, and so the problem would in general have no solution.

Fortunately, as shown above, the governing equation has a special structure at $r = 0$ and the derivative $u'(0)$ can be completely

arbitrary. Therefore, the numerical procedure can in principle start from various values of $u'(0)$ and generate a family of solutions, and then one particular solution can be selected based on the prescribed value u_a at $r = a$. Such an approach could be implemented in the spirit of the shooting method, which converts the problem into a nonlinear algebraic equation $G(\varepsilon_0) = u_a$ where $G(\varepsilon_0)$ is defined as the value of $u(a)$ computed with $u'(0)$ set to ε_0.

The shooting method would require an iterative solution of the nonlinear algebraic equation described above. However, the problem can be solved in a simpler way: The numerical integration procedure can start from $r = a$ and proceed in space in the opposite direction. At $r = a$, the initial value $u(a) = u_a$ is prescribed by the boundary condition, and coefficients $A(u_a, a)$, $B(u_a, a)$ and $C(u_a, a)$ can be evaluated without problems, since formulae (2.37)–(2.39) have no singularity at that point. Therefore, $u'(a)$ can be calculated from (2.33) and a standard integration scheme can be used to construct a numerical solution by marching backwards to $r = 0$. Interestingly, no matter which initial value u_a is imposed at $r = a$, the solution always tends to 0 as the point $r = 0$ is approached. Due to the special structure of the governing equation, different particular solutions have different derivatives $u'(0)$ but the same value $u(0) = 0$.

The most straightforward approach to the numerical solution of differential equation (2.33) can be based on the forward Euler scheme, which needs to be slightly adjusted because we start on the right boundary and proceed to the left. The interval $\langle 0, a\rangle$ is divided into N computational subintervals of size $\Delta r = a/N$, and the numerical approximation of $u(r_i)$ is denoted as u_i, with $r_i = i\Delta r$, $i = N, N-1, \dots, 0$. The procedure starts by setting $r_N = a$ and $u_N = u_a$. In a generic step, the value of u_i is known and the corresponding value of u'_i that approximates $u'(r_i)$ is calculated from Eq. (2.33), using the previously developed procedure that first computes the auxiliary variable η from quadratic equation (2.36). For simplicity, we slightly abuse notation and use u'_i to denote the value of u' at r_i, even though before we used u' with subscripts 1, 2, 3 and 4 to denote four values satisfying Eq. (2.33) at one given point. Now we already know which of these four solutions to choose and subscript i will be used to refer to the computational step number.

Denoting

$$\tilde{r}_i = r_i + u_i \tag{3.1}$$

$$g'_i = g'(\tilde{r}_i) \tag{3.2}$$

$$\alpha_i = \alpha(u_i, r_i) = \frac{\left(1 + \dfrac{u_i}{r_i}\right)^2}{\tilde{r}_i\, g''(\tilde{r}_i)/g'_i - 2 - 2g'^2_i} \tag{3.3}$$

$$A_i = 1 + g'^2_i \tag{3.4}$$

$$B_i = \frac{2\nu u_i}{r_i} + \frac{\nu u_i^2}{r_i^2} - 1 + \nu(1 + g'^2_i)\alpha_i \tag{3.5}$$

$$C_i = \left(\frac{2u_i}{r_i} + \frac{u_i^2}{r_i^2} - \nu\right)\alpha_i \tag{3.6}$$

$$D_i = B_i^2 - 4A_iC_i \tag{3.7}$$

we can express the roots of quadratic Eq. (2.36) as

$$\eta_i^{\pm} = \frac{\pm\sqrt{D_i} - B_i}{2A_i} \tag{3.8}$$

and select the physically meaningful one based on condition (2.61). The corresponding value of displacement derivative is then calculated as

$$u'_i = \sqrt{\eta_i} - 1 \tag{3.9}$$

the value of u_{i-1} is approximated by

$$u_{i-1} = u_i - u'_i\Delta r \tag{3.10}$$

and the algorithm proceeds to the next step, with counter i decremented by 1. It is also possible to directly evaluate the membrane thickness at point r_i, which is according to (2.60) given by

$$h_i = \frac{p}{E} \times \left(-\frac{\tilde{r}_i^2}{r_i g'_i\sqrt{\eta_i}}\right) \times \frac{1}{(1 + g'^2_i)\eta_i - 1} \times \left(1 + \frac{\nu\eta_i}{\alpha_i}\right) \tag{3.11}$$

The forward Euler scheme is simple but leads only to a linear convergence rate. Quadratic convergence can be achieved by the modified forward Euler method, i.e., by treating the value of u'_i as a tentative estimate, from which we construct a mid-step approximation

$$u_{i-1/2} = u_i - u'_i\Delta r/2 \tag{3.12}$$

Then the value of displacement derivative at mid-step, $u'_{i-1/2}$, is computed by using formulae analogous to (3.1)–(3.9) but with subscript i replaced by $i - 1/2$, and with $r_{i-1/2} = r_i - \Delta r/2$. Finally, the displacement at the end of the step is set to

$$u_{i-1} = u_i - u'_{i-1/2}\Delta r \tag{3.13}$$

No matter which integration scheme is adopted, the value of u_0 in the last step does not need to be computed because it is known to be zero. The numerical scheme would lead to values very close to zero. Thickness h_0 cannot be computed from (3.11) because $r_0 = 0$, $\tilde{r}_0 = 0$ and typically also $g'_0 = 0$, which leads to undetermined fractions 0/0 in (3.11) and also in (3.3), needed for the evaluation of α_0. Still, the thickness can be properly evaluated by taking into account that $u'(r)$ tends to a finite limit u'_0 as r tends to zero. In the limit of $r \to 0^+$, formula (2.60) yields

$$h_0 = -\frac{p}{E}\frac{1 - \nu}{(2u'_0 + u'^2_0)g''_0} \tag{3.14}$$

The value of u'_0 can be estimated, e.g., as $2u'_1 - u'_2$.

3.2. Example: Parabolic cap (part II)

The complete solution procedure will be illustrated by an example with the same data as in Section 2.3. The integration process starts from $r_N = a = 9$ mm with the displacement set to $u_N = u_a = 1$ mm. The objective is to obtain a membrane deformed into a parabolic cap with maximum deflection $g_0 = 3$ mm if the membrane is loaded by pressure $p = 0.001\,E$. Poisson's ratio is set to $\nu = 0.4$.

Convergence of the finite difference method is documented in Fig. 2, which shows the displacement function u computed on grids with $\Delta r = 1$ mm, 0.5 mm and 0.25 mm. For reference, a highly accurate solution obtained with $\Delta r = 0.001$ mm is plotted as the solid curve. As expected, the standard forward Euler method (Fig. 2a) gives less accurate results than the modified method (Fig. 2b). In both cases, convergence is regular, but for the standard method the displacements converge from below while for the modified method they converge from above. All subsequent calculations are done with a very fine grid, so that the numerical error remains below the resolution level in presented graphs.

The results plotted in Fig. 2 correspond to the physical solution, with the selection of proper roots η_i that satisfy condition (2.61), and with the derivative u'_i calculated as $\sqrt{\eta_i} - 1$. To demonstrate the consequence of a wrong choice, the graphs in Fig. 3 compare

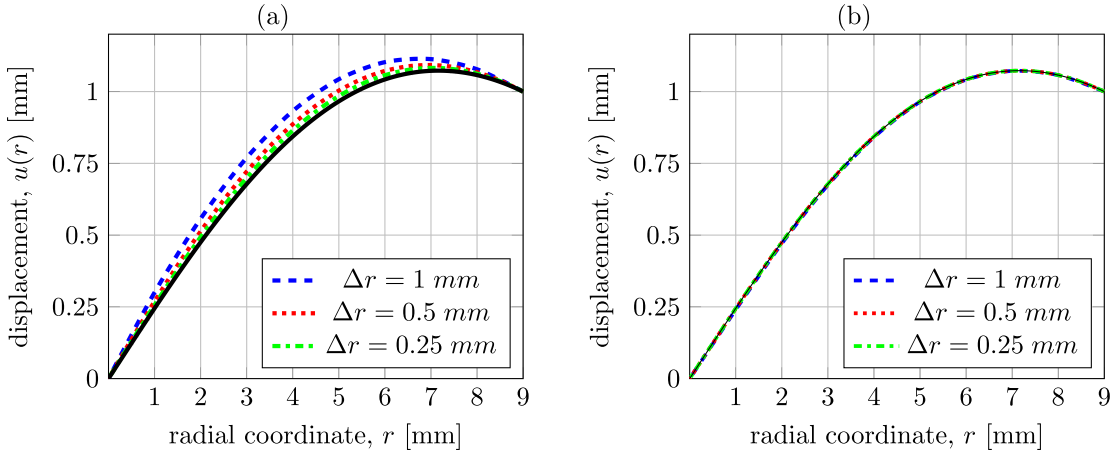

Fig. 2. Illustrative example with $a = 9$ mm, $u_a = 1$ mm, $g_0 = 3$ mm (parabolic cap), $p/E = 10^{-3}$ and $\nu = 0.4$: radial displacements computed on relatively coarse grids using the (a) forward Euler method, (b) modified forward Euler method; the solid curve is an accurate solution obtained with $\Delta r = 0.001$ mm.

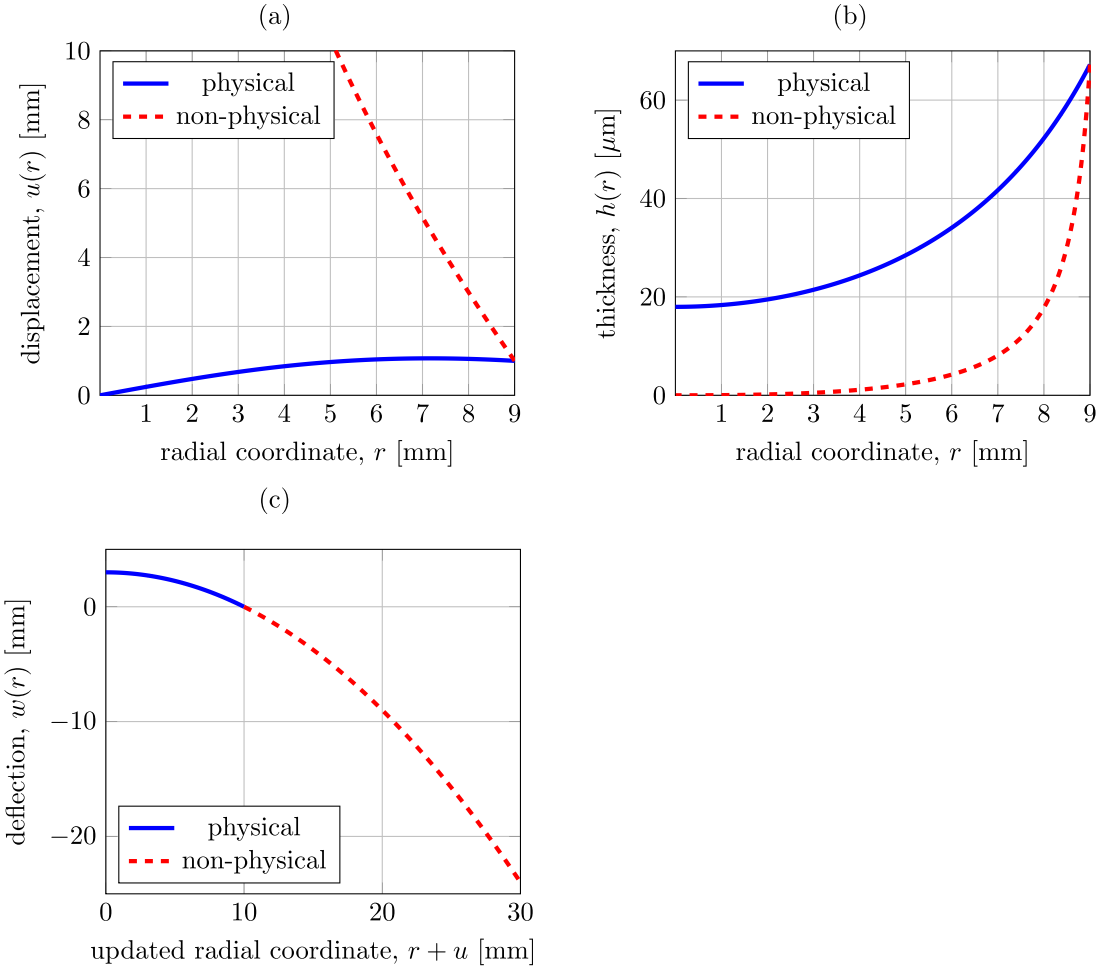

Fig. 3. Results of an illustrative example with $a = 9$ mm, $u_a = 1$ mm, $g_0 = 3$ mm (parabolic cap), $p/E = 10^{-3}$ and $\nu = 0.4$: (a) radial displacements, (b) variable thickness, (c) deformed shape.

the physically meaningful results (solid curves) to non-physical results (dashed curves) that would be obtained with the other root, say η_i^*. In this case, one would need to set $u_i' = -\sqrt{\eta_i^*} - 1$ in order to get a positive membrane thickness, but then $1 + u_i'$ would be negative and the updated radial coordinate $\tilde{r} = r_u$ would become larger than a_p and would grow as r is increased. As the radial coordinate r is decreased and approaches zero, the computed displacement would not tend to zero but grow to infinity (Fig. 3a). The evaluated membrane thickness would be positive but very small compared to the thickness in the physically meaningful case (Fig. 3b). The deformed shapes of the membrane, shown in Fig. 3c, demonstrate that the non-physical solution formally satisfies Eq. (2.33) but points of the deformed membrane would be located on the outer part of the prescribed paraboloid. Of course,

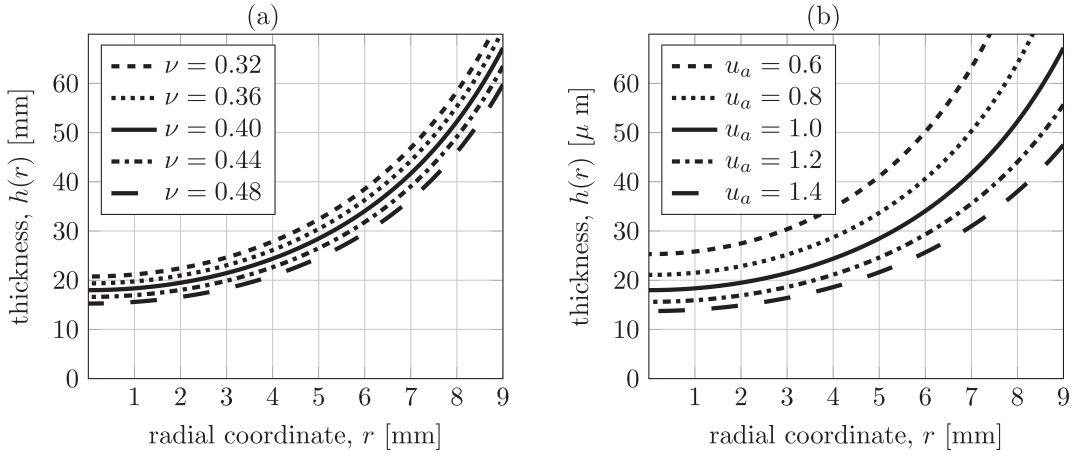

Fig. 4. Influence of (a) Poisson's ratio, (b) prestressing displacement on the optimized membrane thickness distribution; other parameters set to $a = 9$ mm, $g_0 = 3$ mm (parabolic cap) and $p/E = 10^{-3}$.

this configuration could not be attained by continuously increasing the pressure applied on a prestressed circular membrane.

Finally, let us check how the physically meaningful solution is affected by the values of various parameters. The optimal distribution of initial thickness along the radius computed with reference values of parameters is plotted in both parts of Fig. 4 by the thick solid curves. The other curves in Fig. 4a correspond to modified values of Poisson's ratio, and in Fig. 4b they correspond to modified values of initial prestress (expressed in terms of the radial displacement u_a applied on the boundary). The effect of Young's modulus and applied pressure is not shown because the thickness is simply proportional to the ratio p/E. The results in Fig. 4 are plotted for $p/E = 0.001$. If the prescribed maximum deflection g_0 remains the same and the ratio p/E is increased by a factor of 2 (either by doubling the pressure, or by reducing the elastic modulus to one half), the solution in terms of displacement function $u(r)$ remains the same and the membrane thickness must be increased by a factor of 2.

The plots of thickness distribution in Fig. 4 indicate that, in order to get a parabolic cap, the thickness near the border must be larger than near the membrane center. The variation of thickness becomes more dramatic if the prestressing displacement u_a is reduced. The effect of this parameter on the thickness directly at the border, $h(a)$, and at the membrane center, $h(0)$, is further documented in Fig. 5. As expected, for lower prestress the thickness must be larger. If the prestressing displacement tends to zero, the optimized thickness at the center tends to a finite value, but the thickness at the border tends to infinity. For an unprestressed membrane, a solution with bounded thickness cannot be obtained. Of course, in practice the thickness must be kept sufficiently small, otherwise the bending stiffness of the membrane could not be neglected.

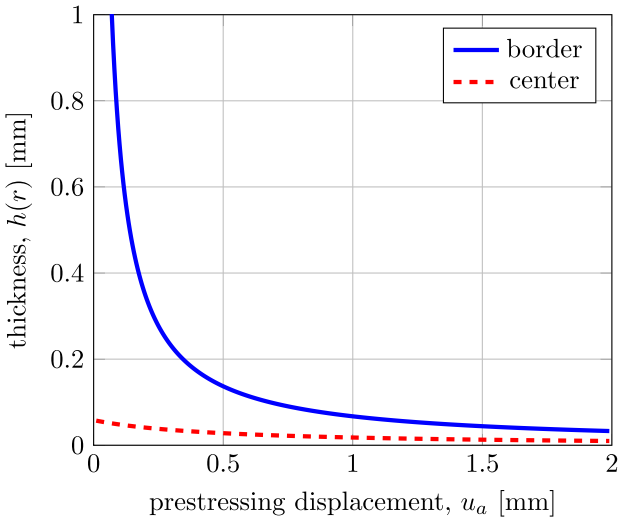

Fig. 5. Optimized values of membrane thickness at the border and at the center depending on the prestressing displacement u_a; other parameters set to $a = 9$ mm, $g_0 = 3$ mm (parabolic cap), $p/E = 10^{-3}$ and $\nu = 0.4$.

4. Analytical solution for spherical cap

Numerical solutions have also been computed for a spherical shape of the deformed membrane, which is described by

$$g(\tilde{r}) = \sqrt{R^2 - \tilde{r}^2} - \frac{a_p^2 - g_0^2}{2g_0} \tag{4.1}$$

where

$$R = \frac{a_p^2 + g_0^2}{2g_0} \tag{4.2}$$

is the radius of the sphere. As usual, $a_p = a + u_a$ is the radius of the membrane in the prestressed state and $g_0 = g(0)$ is the maximum deflection after application of pressure p. It is assumed that $g_0 \leq a_p$, because otherwise the deformed shape would represent more than a half of the full sphere and it could not be described by a unique function g. Differentiation of (4.1) leads to

$$\frac{\mathrm{d}g(\tilde{r})}{\mathrm{d}\tilde{r}} = -\frac{\tilde{r}}{\sqrt{R^2 - \tilde{r}^2}} \tag{4.3}$$

The optimal distribution of membrane thickness has been designed using the numerical procedure described in Section 3.1, and the behavior of the membrane has been checked by finite element simulations performed using the open-source package OOFEM (Patzák, 2012; Patzák and Bittnar, 2001); see Section 5.2 for more details. Based on numerically computed results, it has been found that, in the special case of a spherical cap, the radial strain is equal to the hoop strain (both strains still depend on the radial coordinate). An example is provided in Fig. 6 for a spherical cap with parameters $a = 9$ mm, $u_a = 1$ mm, $g_0 = 3$ mm, $p/E = 10^{-3}$ and $\nu = 0.4$. The thickness has been designed using a computational grid consisting of 9000 equally spaced points, and the same points have been used as finite element nodes. At each integration point of the finite element mesh, the numerically obtained values

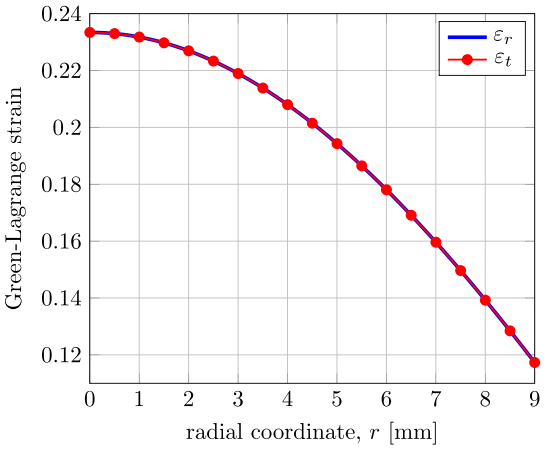

Fig. 6. Radial strain, ε_r, and hoop strain, ε_t, computed numerically for a membrane with variable thickness optimized such that the deformed shape corresponds to a spherical cap; parameters set to $a = 9$ mm, $u_a = 1$ mm, $g_0 = 3$ mm, $p/E = 10^{-3}$ and $\nu = 0.4$.

of the radial strain and of the hoop strain agree up to 5 significant digits. This interesting property of the solution permits an analytical treatment of the governing equations.

The analytical solution is based on the assumption that $\varepsilon_r(r) = \varepsilon_t(r)$ for all $r \in [0, a]$ (this equality is for the moment motivated by numerical results but later will be validated). The assumption of equal strains is equivalent with the assumption of equal stretches, $\lambda_r(r) = \lambda_t(r)$, which can be written in terms of displacements and their derivatives as

$$\sqrt{(1+u')^2 + w'^2} = 1 + \frac{u}{r} \tag{4.4}$$

Substituting

$$w' = (1+u')\,g' = -(1+u')\frac{r+u}{\sqrt{R^2-(r+u)^2}} \tag{4.5}$$

into (4.4) and assuming that $1 + u' > 0$, we obtain

$$(1+u')\frac{R}{\sqrt{R^2-(r+u)^2}} = 1 + \frac{u}{r} \tag{4.6}$$

Introducing a transformed unknown function $\tilde{r}(r) = r + u(r)$ and taking into account that $\tilde{r}'(r) = 1 + u'(r)$, we can rewrite (4.6) in the form

$$\tilde{r}'\frac{R}{\sqrt{R^2-\tilde{r}^2}} = \frac{\tilde{r}}{r} \tag{4.7}$$

This differential equation for unknown function $\tilde{r}(r)$ can be handled by separation of variables, which leads to

$$\frac{R\,\mathrm{d}\tilde{r}}{\tilde{r}\sqrt{R^2-\tilde{r}^2}} = \frac{\mathrm{d}r}{r} \tag{4.8}$$

Integrating on both sides, we obtain

$$\ln\frac{\tilde{r}}{R+\sqrt{R^2-\tilde{r}^2}} = \ln r + C \tag{4.9}$$

where C is an arbitrary constant. After additional easy manipulations, we get the explicit formula

$$\tilde{r}(r) = \frac{2RKr}{1+K^2r^2} \tag{4.10}$$

where $K = \mathrm{e}^C$ is a transformed version of the integration constant.

The value of integration constant K can be determined from the boundary condition $\tilde{r}(a) = a_p$, which leads to the quadratic equation

$$a_p a^2 K^2 - 2RaK + a_p = 0 \tag{4.11}$$

Recall that the sphere radius R is given by (4.2). The discriminant of quadratic equation (4.11) can thus be expressed as

$$D = 4R^2a^2 - 4a_p^2a^2 = 4\left(\frac{(a_p^2+g_0^2)^2}{4g_0^2} - a_p^2\right)a^2 = \frac{(a_p^2-g_0^2)^2}{g_0^2}a^2 \tag{4.12}$$

and it is always non-negative. Consequently, quadratic equation (4.11) has two real roots,

$$K_{1,2} = \frac{2Ra \pm \sqrt{D}}{2a_pa^2} = \frac{\dfrac{a_p^2+g_0^2}{g_0} \pm \dfrac{a_p^2-g_0^2}{g_0}}{2a_pa} = \begin{cases} \dfrac{a_p}{g_0a} \\ \dfrac{g_0}{a_pa} \end{cases} \tag{4.13}$$

and differential equation (4.6) has two solutions,

$$u_{1,2}(r) = \tilde{r}_{1,2}(r) - r = \left(\frac{2RK_{1,2}}{1+K_{1,2}^2r^2} - 1\right)r \tag{4.14}$$

Now we need to determine which of these solutions is physically meaningful. As discussed in Section 2.3, solutions for which $1 + u'(a) < 0$ would lead to a deformed shape that formally satisfies the constraint equation but the membrane is stretched into a region located behind the outer support, and so such solutions should be excluded. It is easy to show that the sign of $1 + u'(a)$ is the same as the sign of $1 - K^2a^2$. Since $1 - K_1^2a^2 = 1 - a_p/g_0$, $1 - K_2^2a^2 = 1 - g_0/a_p$ and g_0 is assumed to be smaller than a_p, we find that a physically meaningful solution is obtained only for $K = K_2 = g_0/(a_pa)$. This solution can be presented in the form

$$u(r) = \left(\frac{2Rg_0a_pa}{a_p^2a^2+g_0^2r^2} - 1\right)r = \left(\frac{(a_p^2+g_0^2)a_pa}{a_p^2a^2+g_0^2r^2} - 1\right)r \tag{4.15}$$

For a given set of parameters, it can be verified that this analytical solution agrees (up to the numerical error) with the numerical solution obtained by the method described in Section 3.1. An example computed with parameters $a = 9$ mm, $a_p = 10$ mm and $g_0 = 3$ mm (leading to $R = 18.1\bar{6}$ mm and $K = 0.0\bar{3}$ mm^{-1}) is presented in Fig. 7a.

Recall that the analytical expression (4.15) for the displacement function u has been constructed in a somewhat heuristic manner, based on the observation that numerical solutions of Eq. (2.33) lead to equal values of radial and circumferential strains. It is therefore necessary to check that the displacement function (4.15) indeed satisfies Eq. (2.33) with function g given by (4.1). Direct substitution would be possible but tedious. Instead of that, we can find expressions for strains, stresses and thickness, and verify the original equilibrium equations (2.17)–(2.18).

First of all, the circumferential stretch and strain can be evaluated from (2.2) and (2.4):

$$\lambda_t = 1 + \frac{u}{r} = \frac{2Rg_0a_pa}{a_p^2a^2+g_0^2r^2} \tag{4.16}$$

$$\varepsilon_t = \tfrac{1}{2}(\lambda_t^2 - 1) = \frac{2R^2g_0^2a_p^2a^2}{(a_p^2a^2+g_0^2r^2)^2} - \frac{1}{2} \tag{4.17}$$

The radial strain, ε_r, could be evaluated independently from (2.1) and (2.3) combined with (4.5), but since the displacement function has been found by solving Eq. (4.6), which corresponds to the equality between the radial and circumferential strains, we can set $\varepsilon_r = \varepsilon_t$ and proceed to the evaluation of stresses

$$\sigma_r = \sigma_t = \frac{E}{1-\nu}\varepsilon_t = \frac{E}{2(1-\nu)}\left(\frac{4R^2g_0^2a_p^2a^2}{(a_p^2a^2+g_0^2r^2)^2} - 1\right) \tag{4.18}$$

based on constitutive equations (2.6)–(2.7).

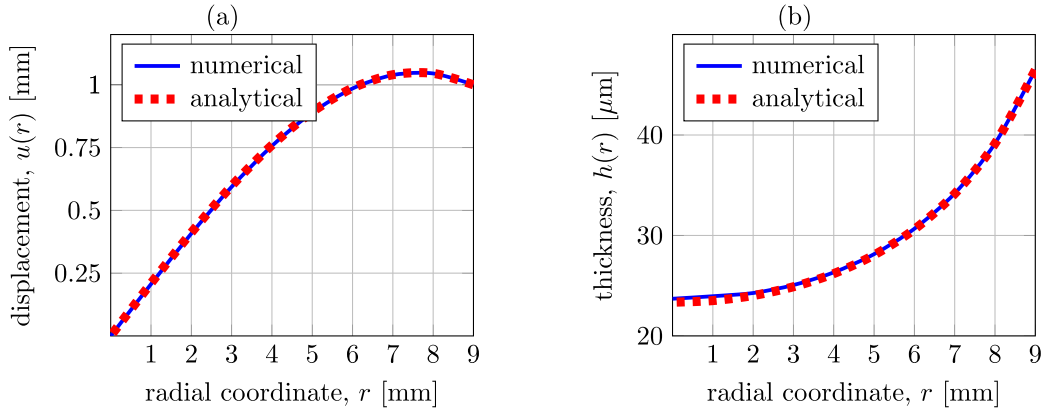

Fig. 7. Example of (a) radial displacement and (b) optimized thickness obtained analytically and numerically for a spherical cap with parameters $a = 9$ mm, $u_a = 1$ mm, $g_0 = 3$ mm, $p/E = 10^{-3}$ and $\nu = 0.4$.

The thickness function, h, could be evaluated from the rather complicated expression (2.34), but since we already have a formula for stress, it is easier to make use of Eq. (2.28). In fact, instead of directly constructing a formula for h, it turns out to be useful to first evaluate

$$\begin{aligned} h\sigma_r &= -\frac{p}{2r}\frac{(r+u)^2}{1+u'}\frac{1}{g'} = \frac{p}{2r}\frac{r+u}{1+u'}\sqrt{R^2-(r+u)^2} \\ &= \frac{p}{2r}\frac{\dfrac{2Rg_0a_par}{a_p^2a^2+g_0^2r^2}}{2Rg_0a_pa\dfrac{a_p^2a^2-g_0^2r^2}{(a_p^2a^2+g_0^2r^2)^2}}\sqrt{R^2-\left(\frac{2Rg_0a_par}{a_p^2a^2+g_0^2r^2}\right)^2} \\ &= \frac{pR}{2} \end{aligned} \tag{4.19}$$

This remarkably simple result means that the product $h\sigma_r$ has a constant value $pR/2$ over the whole membrane, and the same holds for the product $h\sigma_t$ because $\sigma_t = \sigma_r$. It is then easy to write the formula for the thickness,

$$\begin{aligned} h = \frac{pR}{2\sigma_r} &= \frac{(1-\nu)p}{E}\left(\frac{4Rg_0^2a_p^2a^2}{(a_p^2a^2+g_0^2r^2)^2}-\frac{1}{R}\right)^{-1} \\ &= \frac{(1-\nu)p}{2Eg_0}\left(\frac{a_p^2a^2(a_p^2+g_0^2)}{(a_p^2a^2+g_0^2r^2)^2}-\frac{1}{a_p^2+g_0^2}\right)^{-1} \end{aligned} \tag{4.20}$$

For illustration, the optimal distribution of thickness obtained for parameters $a = 9$ mm, $a_p = 10$ mm, $g_0 = 3$ mm, $\nu = 0.4$ and $p/E = 10^{-3}$ is plotted in Fig. 7b. The numerical results shown in the figure have been obtained with a large step $\Delta r = 1$ mm, but they still agree quite well with the analytical solution. The relative error remains below 2%. For sufficiently refined steps, the difference would be indiscernible.

Knowing that $h\sigma_r = h\sigma_t = pR/2 =$ const. and taking into account (4.5), we can reduce equilibrium equations (2.17)–(2.18) to

$$r\left(u'+\frac{u}{r}\right)' = -\frac{2}{R}(r+u)(1+u')\frac{r+u}{\sqrt{R^2-(r+u)^2}} \tag{4.21}$$

$$\left(r(1+u')\frac{r+u}{\sqrt{R^2-(r+u)^2}}\right)' = \frac{1}{R}\big((r+u)^2\big)' \tag{4.22}$$

Relation (4.22) directly follows from (4.6), i.e., from the differential equation from which we determined the displacement function. Making use of (4.6) once again, Eq. (4.21) can be rewritten as

$$\left(u'+\frac{u}{r}\right)' = -\frac{2}{R^2r^2}(r+u)^3 \tag{4.23}$$

and its validity can be confirmed by direct substitution from (4.15). Evaluation of the left-hand side is facilitated by the fact that

$$u'+\frac{u}{r} = \frac{4Rg_0a_p^3a^3}{(a_p^2a^2+g_0^2r^2)^2}-2 \tag{4.24}$$

In summary, it has been demonstrated that the derived closed-form expressions for radial displacement and thickness given by formulae (4.15) and (4.20) lead to an exact satisfaction of the governing differential equations of the problem. This confirms that the assumption of equal strains, $\varepsilon_r(r) = \varepsilon_t(r)$, initially motivated by numerical results, is an exact identity and not just an approximation.

It might seem that the relation $h\sigma_r = h\sigma_t = pR/2$ is something trivial that could have been determined without tedious derivations. Of course, $pR/2$ is the well-known expression for the specific normal force n (considered as force per unit current width) in a spherical membrane of current radius R, uniformly loaded by internal pressure p. For a hollow sphere that has in the undeformed state a spherical shape and constant thickness, it is clear that, due to spherical symmetry, the specific normal force must be the same for all directions, and then the relation $2\pi Rn = \pi R^2 p$, leading to $n = pR/2$, easily follows from equilibrium in the deformed state. On the other hand, in our case the undeformed membrane is flat and its thickness is variable in the undeformed as well as in the deformed state. Moreover, the interpretation of the product $h\sigma_r$ or $h\sigma_t$ as the specific normal force is correct only if $\lambda_r = \lambda_t$, which is indeed the case for the state when the properly designed membrane is loaded precisely into a spherical cap, but not in general.

In the present notation, σ has the meaning of second Piola-Kirchoff stress, and h refers to the membrane thickness in the undeformed state. The normal force per unit width in the undeformed state is the product of h with the first Piola-Kirchhoff normal stress, so it would be equal to $h\lambda_r\sigma_r$ for the radial direction and $h\lambda_t\sigma_t$ for the circumferential direction. The normal force per unit width in the deformed state is the product of the deformed thickness, $h\lambda_3$, with the Cauchy normal stress, which is given by $\sigma_r\lambda_r/(\lambda_t\lambda_3)$ for the radial direction and by $\sigma_r\lambda_t/(\lambda_r\lambda_3)$ for the circumferential direction, with λ_3 denoting the out-of-plane stretch. Only in the special case when $\lambda_r = \lambda_t$, we can interpret $h\sigma_r$ and $h\sigma_t$ as the specific normal forces per unit current width. If they are both equal to $pR/2$ at all points of the membrane midsurface, equilibrium is indeed guaranteed. However, this happens only for the single value of pressure p that was used when designing the membrane. For the same membrane but other values of pressure, the deformed shape will not be precisely spherical. Sensitivity of

the resulting membrane shape to modifications of parameters will be assessed in the next section.

5. Sensitivity to parameters

The boundary value problem derived in Section 2, which can be solved approximately by the numerical method described in Section 3.1, or in some cases even analytically, as demonstrated in Section 4, provides a tool for designing the optimal variation of membrane thickness. The design is optimal in the sense that if the membrane is loaded by a given uniform pressure p, its deflected midsurface perfectly matches a prescribed ideal shape, e.g., a spherical or parabolic cap. Of course, this is true only if the actual properties of the membrane and the actual applied pressure perfectly correspond to the values used in the design procedure. The optimal design is affected by the elastic constants of the membrane, E and ν, by the membrane radius in the undeformed state, a, by the radial displacement on the outer boundary that defines the prestressed state, u_a, and by the desired maximum deflection, g_0. In practice, these parameters are not known exactly, and the purpose of the present section is to examine the sensitivity of the resulting deformed shape to the errors involved in the determination of these material and geometric parameters.

A related issue has already been briefly addressed in Section 3.2, where we studied how changes of certain parameters affect the optimal design. Here we will treat a somewhat different issue, namely how the imprecise knowledge of material properties and prestressing displacement affect the quality of the resulting deformed shape. The basic question can be formulated as follows: If the optimal design is performed using certain assumed values of elastic constants and prestressing displacement but the properties of the actual membrane are different, how much does the actual deformed shape deviate from the desired ideal shape?

It is obvious that if, for instance, the actual elastic modulus of the membrane material is lower than the value used in design, then the membrane deflection caused by the given design pressure will be higher than expected. However, if the main objective is to get as close as possible to the prescribed shape, it makes sense to adjust the pressure such that the maximum deflection would attain the prescribed value. In fact, in many cases one does not control directly the pressure but rather the mass of the fluid that is injected into the device. Provided that the maximum deflection can be measured during the loading process, it is possible to make sure that this deflection will attain the prescribed value, independently of how the actual parameter values differ from those used when designing the thickness distribution.

5.1. Effect of elastic modulus

One general observation that can be made based on the structure of the governing equations is that the designed thickness variation depends on the dimensionless ratio p/E but not on the pressure p and elastic modulus E separately. Indeed, Eq. (2.33) does not contain p and E at all, and Eq. (2.34) contains these parameters only in the form of the fraction p/E. Therefore, if the thickness is designed assuming pressure $p = p_d$ and modulus $E = E_d$ and the actual modulus E_a is different from E_d, it is sufficient to load the membrane by adjusted pressure $p_a = p_d E_a/E_d$ and the design will remain optimal, i.e., the deformed shape will exactly correspond to the desired one. In other words, an imprecise knowledge of the elastic modulus can be fully compensated by adjusting the applied pressure, making sure that the maximum deflection attains the prescribed value. This is true for an arbitrary ideal shape, because Eqs. (2.33)–(2.34) are general and have the same form for an arbitrary shape function g.

5.2. Effect of Poisson's ratio

The effect of Poisson's ratio is more difficult to assess. Eqs. (2.33)–(2.34) contain Poisson's ratio, ν, which multiplies certain terms and is not combined with any other parameter that could be adjusted so as to compensate the effect of imprecise knowledge of ν. Therefore, in general it can be expected that if the design is based on an assumed value of ν that differs from the actual one, the actual deformed shape will deviate from the ideal shape even if the pressure is adjusted to get the prescribed maximum deflection. To assess how important this deviation is, we have performed numerical simulations of the deformed membrane, using the finite element method with axisymmetric membrane elements based on linear interpolation of both displacement components, as described in our previous paper (Pokorný et al., 2017a). The calculations have been done within the OOFEM open-source package (Patzák, 2012; Patzák and Bittnar, 2001).

First of all, it is good to check that loading of an optimally designed membrane with all parameters kept the same as in the design indeed leads to the desired deformed shape. This simulation also represents an independent verification of the design procedure because the deflection is now evaluated by a different numerical technique. The objective is to determine the numerical error in the case when the theoretical result would be expected to be perfect. In general, the numerical error comes from the design procedure that defines the thickness distribution (performed numerically using the algorithm described in Section 3.1) as well as from the finite element solution of the membrane deflection. To isolate the second source of error, let us first consider the **spherical cap**, for which the optimal thickness distribution is described by an analytical formula. The calculations are done with parameter values considered in the previous examples, i.e., $a = 9$ mm, $g_0 = 3$ mm, $p/E = 10^{-3}$, $\nu = 0.4$ and $u_a = 1$ mm. The ideal shape is described by function g given in (4.1), with $a_p = a + u_a = 10$ mm and $R = (a_p^2 + g_0^2)/(2g_0) = 18.1\bar{6}$ mm. The optimum thickness distribution is evaluated analytically from (4.20), and the exact value of h is computed at each Gauss integration point of the finite element model, which uses 2 integration points per element. Local deviations from the optimal spherical shape along the membrane radius are plotted by blue solid curves in Fig. 8a-c for simulations with 90, 900 and 9000 finite elements. Already for 90 elements, the deviation of the computed surface from the ideal shape does not exceed 400 nm, and for 900 elements it is in the order of a few nanometers.

To characterize the deviation by one global quantity, the root-mean-square error is defined as

$$e_{RMS} = \left(\frac{1}{a_p} \int_0^a [w(r) - g(r + u(r))]^2 \big(1 + u'(r)\big)\, \mathrm{d}r \right)^{1/2} \tag{5.1}$$

where u and w are the displacement components computed by finite elements. The dependence of this error on the number of finite elements is plotted by the red dashed curve in Fig. 8d. As the number of elements increases, the error tends to zero and is roughly proportional to the square of the element size, as may have been expected. Here, the error comes exclusively from the finite element simulation of the deformed shape, and the "actual" deformed shape obtained in the limit would be an ideal spherical cap. It is thus confirmed that the proposed method provides excellent designs, and if the membrane could indeed be manufactured with the assumed properties and loaded in the prescribed way, the final deformed shape would be perfect.

As the next step, we repeat the calculations for the **parabolic cap** described by formula (2.43), with all geometric and material parameters kept the same as before. No analytical expression for the optimal thickness is available, and so the thickness needs to be calculated numerically, which introduces an additional error. In

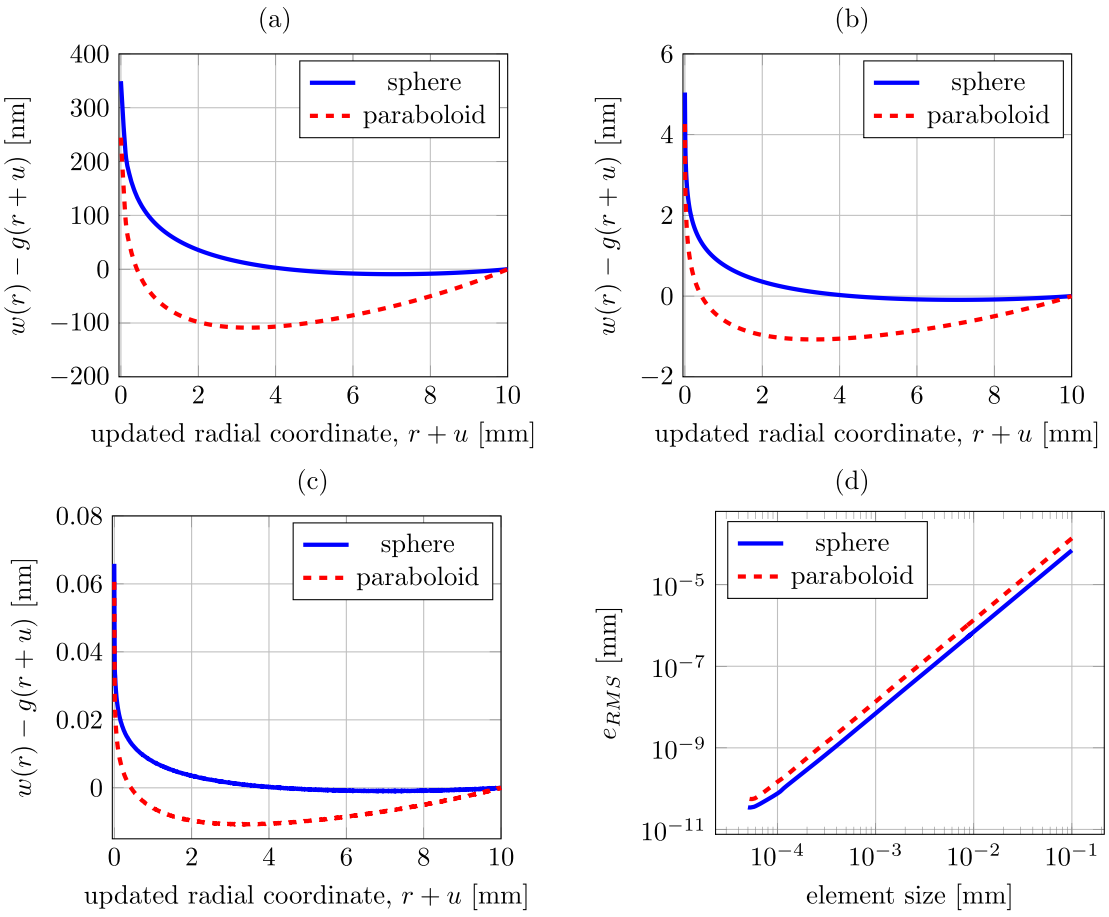

Fig. 8. Deviation of the numerically computed deflected shape from the ideal shape for simulations with (a) 90, (b) 900 and (c) 9000 finite elements; (d) dependence of the root-mean-square error on the element size.

all simulations, we use grid points for thickness evaluations coincident with finite element nodes, and the designed values of thickness calculated at the grid points are transmitted to the integration points of finite elements by linear interpolation. Local deviations from the optimal parabolic shape along the membrane radius for simulations with 90, 900 and 9000 finite elements and the dependence of the global root-mean-square error on the number of elements are plotted by dashed red curves in Fig. 8a-c. The deviations are slightly larger than for the spherical cap, which is caused by an additional error due to the numerical design of optimal thickness. Nevertheless, the error is again roughly proportional to the square of finite element size (equal to the grid spacing) and tends to zero as the mesh and grid are simultaneously refined.

The foregoing simulations show that the numerical error caused by the combined effect of numerical evaluation of optimal thickness and finite element simulation of the deflected shape is, for the reference set of parameters, in the order of nanometers if 900 elements (and the same number of grid intervals) are used. Now we proceed to the evaluation of the effect of Poisson's ratio. The thickness design is done for $\nu_d = 0.4$, as before, but the deflected shape is simulated for membranes with actual Poisson ratios $\nu_a = 0.36$ and 0.44. The applied pressure is adjusted to get the prescribed maximum deflection, $g_0 = 3$ mm, and 900 elements are used.

For the **parabolic cap**, the resulting deviations from the ideal shape are in the order of micrometers, i.e., by three orders of magnitude larger than if the actual Poisson ratio is set equal to the value used in design; see Fig. 9a. Moreover, if the number of finite elements (and simultaneously of the grid intervals) is increased to 9000, the error is not visibly reduced. This indicates that the shape distortion is caused by the deviation of the actual Poisson ratio from the value used in design. Still, from the practical point of view, the deviation from the ideal shape is relatively small, with the maximum local deviation of about 0.07% of the maximum deflection and the root-mean-square error below 0.05% of the maximum deflection, even though the change of Poisson's ratio from 0.4 to 0.36 or to 0.44 is quite large. Additional numerical simulations with other values of Poisson's ratio reveal that the deviation is roughly proportional to the difference between the actual value of Poisson's ratio and the value used in design of optimal thickness distribution. For the reference case, the root-mean-square error can be estimated as $e_{RMS} \approx |\nu_a - \nu_d| \times 35\ \mu$m, where $\nu_d = 0.4$ is the design value of Poisson's ratio and ν_a is the actual one; see Fig. 9b.

An interesting result is obtained for the **spherical cap**. Even after a change of Poisson's ratio, the calculated error is of the same order of magnitude as for the original value of ν, i.e., in the order of nanometers if 900 elements are used, and it keeps decreasing with increasing number of elements (provided that the applied pressure is always adjusted so as to get the prescribed value of maximum deflection). This indicates that the error is purely numerical and vanishes in the limit. The design remains optimal even after a change of Poisson's ratio. The reason becomes clear if we examine formula (4.20) for the optimal thickness, in which a function dependent purely on the geometrical parameters g_0, a_p and a is multiplied by the fraction $(1-\nu)p/E$. This means that, for the spherical cap, inaccurate knowledge of both elastic constants can be fully compensated by adjusting the applied pressure. For the elastic modulus, a similar statement holds independently of the

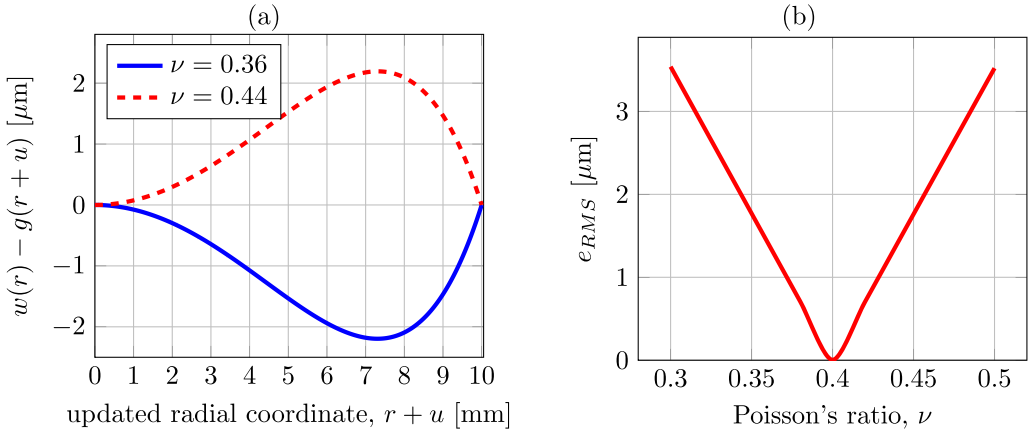

Fig. 9. Influence of Poisson's ratio ν on the deviation from the ideal parabolic shape: (a) deviation of deflections along the radius for $\nu = 0.36$ and 0.44, (b) dependence of the root-mean-square error on Poisson's ratio in the range from 0.3 to 0.5.

prescribed shape; see Section 5.1. The extension to Poisson's ratio is valid for the spherical cap only.

It may seem strange that Eq. (2.33), from which the radial displacement u is calculated, contains parameter ν, but the analytical solution (4.15) valid for the spherical cap is independent of ν. The only possible explanation is that the solution of the reduced version of (2.33) obtained for $\nu = 0$ automatically satisfies the full equation for any other ν, i.e., the expression that multiplies ν on the left-hand side of (2.33) vanishes if the solution of the reduced equation with $\nu = 0$ is substituted. The reduced equation reads

$$\frac{(r+u)^2}{2r^2g'}\left(\frac{u}{r}+\frac{u^2}{2r^2}\right)+(1+u')^2\left(\frac{(r+u)g''}{2g'^2}-\frac{1}{g'}-g'\right)$$
$$\left(u'+\tfrac{1}{2}u'^2+\tfrac{1}{2}(1+u')^2g'^2\right)=0 \tag{5.2}$$

and the condition that the complementary terms that are multiplied by ν vanish can be written as

$$(1+u')^2\left(\frac{(r+u)g''}{2g'^2}-\frac{1}{g'}-g'\right)\left(\frac{u}{r}+\frac{u^2}{2r^2}\right)+\frac{(r+u)^2}{2r^2g'}$$
$$\left(u'+\tfrac{1}{2}u'^2+\tfrac{1}{2}(1+u')^2g'^2\right)=0 \tag{5.3}$$

To prove that if function u satisfies (5.2) then it also automatically satisfies (5.3), it is sufficient to show that

$$\frac{u}{r}+\frac{u^2}{2r^2}=u'+\tfrac{1}{2}u'^2+\tfrac{1}{2}(1+u')^2g'^2 \tag{5.4}$$

which can be rewritten as

$$\left(1+\frac{u}{r}\right)^2=(1+u')^2(1+g'^2) \tag{5.5}$$

This is found to be equivalent with Eq. (4.4) in which w' is replaced by $(1+u')g'$, as indicated in (4.5). Therefore, condition (5.4) corresponds to the differential equation from which the analytical solution for u was constructed in Section 4, and so it is natural that this condition is indeed satisfied. Of course, the validity of (5.4) could also be checked by directly substituting u given by (4.15) and g' given by (4.3).

5.3. Effect of prestressing displacement

In the preceding subsection we have examined how imprecise knowledge of the actual elastic constants affects the quality of the resulting deformed membrane shape. Another important parameter that may play a role is the initial radial displacement that induces prestress before the membrane is loaded by liquid pressure. The optimal design is based on an assumed value of u_a, but the actually imposed displacement may slightly differ because technically it is quite difficult to impose precisely the prescribed value of the displacement on the boundary (especially since this displacement is taken with respect to the undeformed state of a very flexible membrane). Therefore, it is of interest to look at deviations from an ideal shape caused by changes of the actually prescribed displacement.

Of course, if the actually imposed radial displacement $u_a + \Delta u_a$ differs from the value u_a that was used in the design stage, the deformed shape must differ from the originally prescribed one, even if the pressure is adjusted such that the maximum deflection attains the prescribed value. The reason is that the original shape was supposed to have zero deflection at a circular boundary of radius $a + u_a$ but the actual boundary is now a circle of radius $a + u_a + \Delta u_a$. Instead of evaluating the deviation from the originally intended shape, we can take as a reference an ideal shape of the same type (a spherical or parabolic cap) but with adjusted parameters. For instance, if the originally intended shape was a spherical cap of a certain radius, the actual shape could be close to a spherical cap with a somewhat different radius.

The effect of prestressing displacement is illustrated by a numerically computed example, with the design of thickness distribution performed for a spherical or parabolic cap with the standard set of parameters used in previous examples. In particular, the radius of the undeformed membrane is taken as $a = 9$ mm and the prestressing displacement is in the design stage considered as $u_a = 1$ mm. The actual deformed shape is then computed by finite elements for prescribed displacements equal to 0.9 mm and 1.1 mm. In each case, the applied pressure is adjusted so as to produce the desired value of maximum deflection, $g_0 = 3$ mm. When evaluating the deviation, the ideal shape is taken as a spherical or parabolic cap characterized by g_0 as initially prescribed and by a_p equal to the actual value, i.e., 9.9 mm or 10.1 mm. Deviations from such adjusted ideal shapes are plotted in Fig. 10. It is worth noting that even though the prestressing displacement has been changed by $\pm$ 10%, deviations from the adjusted ideal shape (perfect sphere or perfect paraboloid) are still by three orders of magnitude smaller than the maximum deflection. In this sense, the optimum design can be considered as relatively robust, not too sensitive to imprecise enforcement of the actual prestressing displacement. This conclusion is confirmed by Fig. 11, which shows that when the prestressing displacement is varied between 0.5 mm and 2.0 mm, the root-mean-square error remains below 28 μm for the parabolic cap and below 15 μm for the spherical cap, i.e., it does not exceed 1% of the maximum deflection.

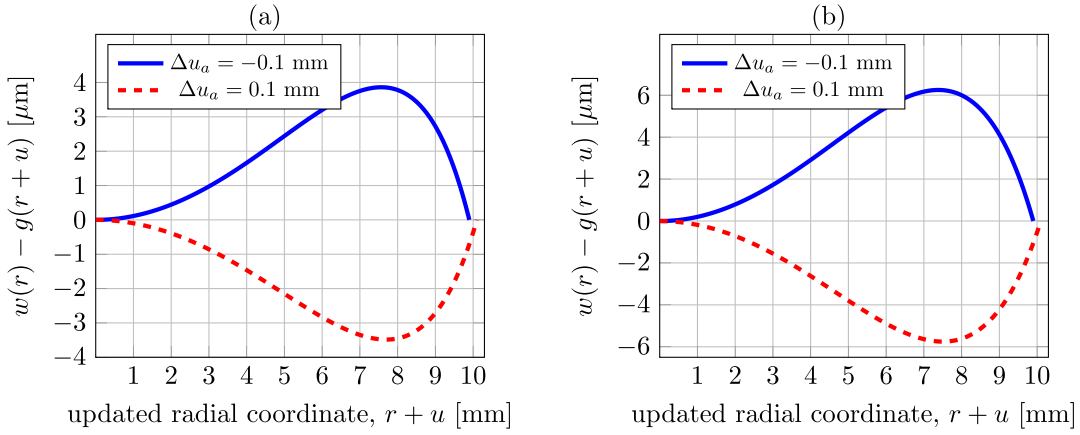

Fig. 10. Influence of prestressing displacement on the deviation from the ideal shape: (a) for a spherical cap, (b) for a parabolic cap.

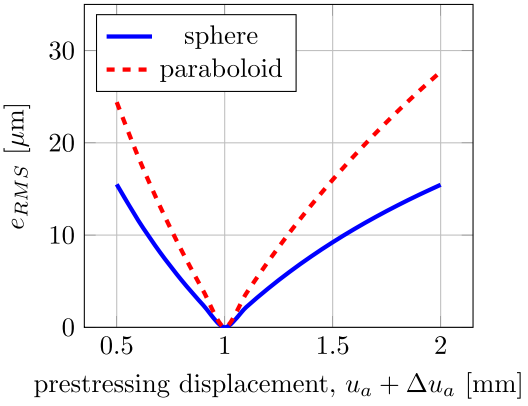

Fig. 11. Dependence of the root-mean-square error on prestressing displacement $u_a + \Delta u_a$ in the range from 0.5 to 2.0 mm.

6. Summary and conclusions

We have studied the mechanical behavior of axially symmetric elastic membranes that are first prestressed by imposing a radial displacement on the boundary and then subjected to a uniform hydrostatic pressure acting perpendicular to the deformed midsurface. The membrane material has been described by the Saint Venant-Kirchhoff material law, which provides a good approximation of the actual response of materials used for membranes in liquid lenses. The primary objective has been to develop techniques for design of variable thickness such that the deformed membrane would have a prescribed shape, e.g., a spherical or parabolic cap. The main conclusions can be summarized as follows:

- Under the given assumptions, the problem of optimum thickness design can be reduced to one nonlinear first-order differential equation for the radial displacement. Once this equation is solved, the corresponding thickness distribution can be evaluated by substitution into an algebraic expression.
- Formally, the solution of the governing first-order equation should satisfy two boundary conditions. However, the condition of zero radial displacement on the axis of symmetry is satisfied "automatically" due to the special asymptotic structure of the governing equation. Effectively, only one boundary condition that prescribes the displacement on the outer boundary needs to be enforced.
- Due to the implicit form of the governing equation, the solution is not unique. For a given value of displacement at a given point, there are in general four possible values of the displacement derivative that satisfy the governing equation. However, only one of them leads to a physically admissible solution.
- A numerical algorithm based on a finite difference scheme has been developed for problems with an arbitrary shape of the prescribed deformed midsurface. Robustness and accuracy of this algorithm has been tested for prescribed surfaces that have the shape of a parabolic or spherical cap.
- The resulting distributions of membrane thickness continuously increase from the minimum value on the axis of symmetry to the maximum value on the outer boundary. They are strongly affected by the applied prestress. As the prestress is reduced to zero, the maximum thickness tends to infinity. Therefore, a certain minimum level of prestress is needed in order to keep the designed thickness physically realistic.
- For the special but practically important case of a spherical cap, an analytical solution for the optimum thickness distribution and for the displacements has been derived.
- It has been verified by finite element simulations that the optimally designed membranes indeed deform into the prescribed shape, provided that the material and geometric properties are the same as assumed in the design.
- Sensitivity to elastic constants and to the prescribed prestressing displacement has been studied analytically and numerically. If the actually applied pressure is adjusted so as to attain the prescribed value of the maximum deflection, the deformed shape exactly corresponds to the desired one even if the actual elastic modulus differs from the value assumed in design. This is true for an arbitrary shape. For the special case of a spherical shape, an analogous statement holds also for changes of Poisson's ratio.
- Sensitivity to changes of Poisson's ratio for a parabolic cap and to changes of prestressing displacement for parabolic and spherical caps has been evaluated and shown to be relatively mild. Therefore, the optimal thickness design remains useful even if the properties are not known in advance with absolute accuracy.

The developed thickness design procedure can be used for further analyses and simulations of imaging properties of the resulting optical elements. It would also be interesting to validate the obtained results experimentally. The numerical procedure and the analytical solution can serve for the development of high-precision optical elements.

If the designed thickness of the membrane is not sufficiently small, the solution may require additional corrections that remove certain simplifying assumptions. First, it should be taken into ac-

count that the optical surface is actually the top surface of the membrane (at contact with air) rather than the midsurface. Second, flexural stiffness may become important, especially near the clamped edge. These refinements are the subject of an ongoing research.

Declaration of Competing Interest

The authors declare that they have no known competing financial interests or personal relationships that could have appeared to influence the work reported in this paper.

Acknowledgements

The first and third authors acknowledge financial support received from the European Regional Development Fund through the Center of Advanced Applied Sciences at the Czech Technical University in Prague (project No. CZ.02.1.01/0.0/0.0/16_019/0000778). The second author has received financial support from the Czech Technical University in Prague (internal projects No. SGS18/105/OHK1/2T/11 and SGS19/105/OHK1/2T/11).

Supplementary material

Supplementary material associated with this article can be found, in the online version, at doi:10.1016/j.ijsolstr.2020.04.021.

References

Allman, D., 1982. Variational solutions for the nonlinear deflexion of an annular membrane under axial load. Int. J. Mech. Sci. 24 (12), 749–753. doi:10.1016/0020-7403(82)90025-X.

Audoly, B., Pomeau, Y., 2010. Elasticity and Geometry: From Hair Curls to the Nonlinear Response of Shells. OUP Oxford.

Campbel, J.D., 1956. On the theory of initially tensioned circular membranes subjected to uniform pressure. Q. J. Mech. Appl.Math. 9 (1). doi:10.1093/qjmam/9.1.84.

Choi, H., Han, D.S., Won, Y.H., 2011. Adaptive double-sided fluidic lens of polydimethylsiloxane membranes of matching thickness. Opt. Lett. 36 (23), 4701–4703. doi:10.1364/OL.36.004701.

Ding, Z., Wang, C., Hu, Z., Cao, Z., Zhou, Z., Chen, X., Chen, H., Qiao, W., 2017. Surface profiling of an aspherical liquid lens with a varied thickness membrane. Opt. Express 25 (4), 3122–3132. doi:10.1364/OE.25.003122.

Du, J.-W., Wang, X.-Y., Liang, D., 2016. Bionic optical imaging system with aspheric solid-liquid mixed variable-focus lens. Opt. Eng. 55 (2), 23105. doi:10.1117/1.OE.55.2.023105.

Fichter, W., 1997. Some Solutions for the Large Deflections of Uniformly Loaded Circular Membranes. National Aeronautics and Space Administration, Langley Research Center.

Fuh, Y.-K., Lin, M.-X., Lee, S., 2012. Characterizing aberration of a pressure-actuated tunable biconvex microlens with a simple spherically-corrected design. Opt. Lasers Eng. 50 (12), 1677–1682. doi:10.1016/j.optlaseng.2012.07.013.

Fuh, Y.-K., Ming-XinLin, ShyongLee, 2012. Characterizing aberration of a pressure-actuated tunable biconvex microlens with a simple spherically-corrected design. Opt. Lasers Eng. 50, 1677–1682. doi:10.1016/j.optlaseng.2012.07.013.

Goldberg, M.A., Pifko, A.B., 1963. Large deflection analysis of uniformly loaded annular membranes. AIAA J. 1, 2111–2115.

Hasan, N., Banerjee, A., Kim, H., Mastrangelo, C.H., 2017. Tunable-focus lens for adaptive eyeglasses. Opt. Express 25 (2), 1221–1233. doi:10.1364/OE.25.001221.

Hencky, H., 1915. On the stress state in circular plates with vanishing bending stiffness. Z. Math. Phys. 63, 311–317.

Holochip. http://www.holochip.com.

Huang, H., Wei, K., Wang, Q., Zhao, Y., 24 March 2016. Improved optical resolution for elastomer-liquid lens at high diopter using varied thickness membrane. In: Proc. SPIE 9705, Microfluidics, BioMEMS, and Medical Microsystems XIV, p. 970504. doi:10.1016/j.ijleo.2013.01.022.

Johnston, I.D., McCluskey, D.K., Tan, C.K.L., Tracey, M.C., 2014. Mechanical characterization of bulk Sylgard 184 for microfluidics and microengineering. J. Micromech. Microeng. 24 (3), 35017. doi:10.1088/0960-1317/24/3/035017.

Kao, R., Perrone, N., 1971. Large deflections of axisymmetric circular membranes. Int. J. Solids Struct. 7 (12), 1601–1612. doi:10.1016/0020-7683(71)90001-1.

Kelkar, A., Elber, W., Raju, I., 1985. Large deflections of circular isotropic membranes subjected to arbitrary axisymmetric loading. Comput. Struct. 21 (3), 413–421. doi:10.1016/0045-7949(85)90118-X.

Li, L., Wang, Q.-H., Jiang, W., 2011. Liquid lens with double tunable surfaces for large power tunability and improved optical performance. J. Opt. 13 (11), 115503.

Liang, D., Wang, X.-Y., 2016. A bio-inspired optical system with a polymer membrane and integrated structure. Bioinspir. Biomimet. 11 (6), 66008.

Mikš, A., Novák, J., Novák, P., 2013. Algebraic and numerical analysis of imaging properties of thin tunable-focus fluidic membrane lenses with parabolic surfaces. Appl. Opt. 52 (10), 2136–2144. doi:10.1364/AO.52.002136.

Mikš, A., Novák, P., 2014. Calculation of a surface shape of a pressure actuated membrane liquid lens. Opt. Lasers Eng. 58, 60–66. doi:10.1016/j.optlaseng.2014.01.026.

Optotune. http://www.optotune.com.

Patzák, B., 2012. OOFEM - an object-oriented simulation tool for advanced modeling of materials and structures. Acta Polytech. 52 (6), 59–66.

Patzák, B., Bittnar, Z., 2001. Design of object oriented finite element code. Adv. Eng. Softw. 32 (10–11), 759–767.

Perrone, N., Kao, R., 1971. A general nonlinear relaxation technique for solving nonlinear problems in mechanics. J. Appl. Mech. 38, 371–376.

Pifko, A.B., Goldberg, M.A., 1964. Iterative and power series solutions for the large deflection of an annular membrane. AIAA J. 2, 1340–1342.

Pokorný, P., Šmejkal, F., Kulmon, P., Novák, P., Novák, J., Mikš, A., Horák, M., Jirásek, M., 2017. Calculation of nonlinearly deformed membrane shape of liquid lens caused by uniform pressure. Appl. Opt. 56 (21), 5939–5947.

Pokorný, P., Šmejkal, F., Kulmon, P., Novák, P., Novák, J., Mikš, A., Horák, M., Jirásek, M., 2017. Deformation of a prestressed liquid lens membrane. Appl. Opt. 56 (34), 9368–9376.

Rawicz, A.H., Mikhailenko, I., 1996. Modeling a variable-focus liquid-filled optical lens. Appl. Opt. 35 (10), 1587–1589. doi:10.1364/AO.35.001587.

Ren, H., Wu, S., 2012. Introduction to Adaptive Lenses. Wiley Series in Pure and Applied Optics. Wiley.

Ren, H., Wu, S.-T., 2007. Variable-focus liquid lens. Opt. Express 15 (10), 5931–5936. doi:10.1364/OE.15.005931.

Santiago-Alvarado, A., Gonzlez-Garca, J., Itubide-Jimnez, F., Campos-Garca, M., Cruz-Martinez, V., Rafferty, P., 2013. Simulating the functioning of variable focus length liquid-filled lenses using the finite element method (FEM). Optik 124 (11), 1003–1010. doi:10.1016/j.ijleo.2013.01.022.

Shaw, D., Lin, C.-W., 2007. Design and analysis of an asymmetrical liquid-filled lens. Opt. Eng. 46 (12), 123002–123002–8. doi:10.1117/1.2821426.

Sheploak, M., Dugundji, J., 1998. Large deflections of clamped circular plates under initial tension and transitions to membrane behavior. J. Appl. Mech. 65 (1).

Stanford, B., Ifju, P., 2008. The validity range of low fidelity structural membrane models. Exp. Mech. 48 (6), 697. doi:10.1007/s11340-008-9152-2.

Sugiura, N., Morita, S., 1993. Variable-focus liquid-filled optical lens. Appl. Opt. 32 (22), 4181–4186. doi:10.1364/AO.32.004181.

Sylgard 184 Silicone Elastomer Kit. http://www.dowcorning.com/applications/search/products/Details.aspx?prod=01064291.

Timoshenko, S., Woinowsky-Krieger, S., 1959. Theory of plates and shells. Engineering Societies Monographs. McGraw-Hill.

Volmir, A., 1967. Flexible Plates and Shells. Air Force Flight Dynamics Laboratory, Research and Technology Division, Air Force Systems Command.

Wang, L., Oku, H., Ishikawa, M., 2013. Development of variable-focus lens with liquid-membrane-liquid structure and 30 mm optical aperture. Proc. SPIE 8617, 861706–861706–7. doi:10.1117/12.2005531.

Wang, L., Oku, H., Ishikawa, M., 2014. An improved low-optical-power variable focus lens with a large aperture. Opt. Express 22 (16), 19448–19456. doi:10.1364/OE.22.019448.

Yang, Q., Kobrin, P., Seabury, C., Narayanaswamy, S., Christian, W., 2008. Mechanical modeling of fluid-driven polymer lenses. Appl. Opt. 47 (20), 3658–3668. doi:10.1364/AO.47.003658.

Zhang, D.-Y., Justis, N., Lien, V., Berdichevsky, Y., Lo, Y.-H., 2004. High-performance fluidic adaptive lenses. Appl. Opt. 43 (4), 783–787. doi:10.1364/AO.43.000783.

Zhao, P., Çağlar Ataman, Zappe, H., 2015. Spherical aberration free liquid-filled tunable lens with variable thickness membrane. Opt. Express 23 (16), 21264–21278. doi:10.1364/OE.23.021264.